Renormalization of stochastic lattice models: Epitaxial surfaces

Christoph A. Haselwandter
Department of Physics, Massachusetts Institute of Technology, Cambridge, Massachusetts 02139, USA

Dimitri D. Vvedensky
The Blackett Laboratory, Imperial College London, London SW7 2BW, United Kingdom
(Received 28 December 2007; published 20 June 2008)

We present the application of a method [C. A. Haselwandter and D. D. Vvedensky, Phys. Rev. E **76**, 041115 (2007)] for deriving stochastic partial differential equations from atomistic processes to the morphological evolution of epitaxial surfaces driven by the deposition of new material. Although formally identical to the one-dimensional (1D) systems considered previously, our methodology presents substantial additional technical issues when applied to two-dimensional (2D) surfaces. Once these are addressed, subsequent coarse-graining is accomplished as before by calculating renormalization-group (RG) trajectories from initial conditions determined by the regularized atomistic models. Our applications are to the Edwards-Wilkinson (EW) model [S. F. Edwards and D. R. Wilkinson, Proc. R. Soc. London, Ser. A **381**, 17 (1982)], the Wolf-Villain (WV) model [D. E. Wolf and J. Villain, Europhys. Lett. **13**, 389 (1990)], and a model with concurrent random deposition and surface diffusion. With our rules for the EW model no appreciable crossover is obtained for either 1D or 2D substrates. For the 1D WV model, discussed previously, our analysis reproduces the crossover sequence known from kinetic Monte Carlo (KMC) simulations, but for the 2D WV model, we find a transition from smooth to unstable growth under repeated coarse-graining. Concurrent surface diffusion does not change this behavior, but can lead to extended transient regimes with kinetic roughening. This provides an explanation of recent experiments on Ge(001) with the intriguing conclusion that the same relaxation mechanism responsible for ordered structures during the early stages of growth also produces an instability at longer times that leads to epitaxial breakdown. The RG trajectories calculated for concurrent random deposition and surface diffusion reproduce the crossover sequences observed with KMC simulations for all values of the model parameters, and asymptotically always approach the fixed point corresponding to the equation proposed by Villain [J. Phys. I **1**, 19 (1991)] and by Lai and Das Sarma [Phys. Rev. Lett. **66**, 2899 (1991)]. We conclude with a discussion of the application of our methodology to other growth settings.

DOI: 10.1103/PhysRevE.77.061129 PACS number(s): 05.40.−a, 81.15.Aa, 05.10.Gg

I. INTRODUCTION

Surfaces driven by the deposition of material have become a paradigm for nonequilibrium phenomena. A standard example of this scenario is molecular-beam epitaxy (MBE) [1–6], wherein a crystalline film is formed on an underlying crystalline substrate as the result of the deposition of new material from a molecular beam. The simplest experimental realization of MBE is homoepitaxial growth, in which the substrate and film are the same material. Precise control over sample preparation and growth conditions and the availability of *in situ* and *ex situ* imaging techniques, often with atomic-scale resolution, have fostered a huge literature on the application of MBE to various materials systems and accompanying theories with various levels of sophistication [7].

MBE is a two-step process carried out in an ultrahigh vacuum environment [8]. In the first step, the constituents of the growing film are delivered ballistically onto a heated substrate as atoms or simple homoatomic molecules (e.g., atomic Ga and either As_2 or As_4 for GaAs, or atomic Si for Si). The second step is the migration of these deposited species on the surface prior to their incorporation into the growing material or, possibly, their desorption from the surface. The morphology of the growing film is thereby determined by the competing effects of the deposition process, which drives the surface away from equilibrium, and the relaxation of the surface profile toward equilibrium through surface diffusion [9]. Thus, at low temperatures and/or high fluxes, nonequilibrium effects dominate the growth process, while thermodynamics becomes more effective at high temperatures and/or low fluxes.

In common with other growth scenarios [10–12] and a variety of other nonequilibrium systems [13–18], MBE is often modeled by transition rules for site occupancies on a lattice that are designed to capture the essence of atomic-scale interactions. The basic approach is to replace the *deterministic* equations used in first-principles computations of MBE, whose time steps are determined by atomic vibrational frequencies, by *stochastic* transition rates for slower atomistic processes such as adatom hopping [19,20]. As a result, all details regarding the underlying mechanism of a given kinetic process are lost and atomic trajectories are replaced by instantaneous transitions between different lattice states. An appealing property of such lattice models is that, if derived from first-principles descriptions, they are self-regulating in the sense that infrequent processes, for which the corresponding transition times are very large compared to experimental time scales, can be easily identified and eliminated. Thus, there is a natural basis for distinguishing between "relevant" and "irrelevant" processes. From a computational perspective, lattice models circumvent the "time gap" problem of infrequent events [20] that can severely restrict the applicability of first-principles methods in MBE.

The transition rates in lattice models for surface growth can be of purely phenomenological nature [10–12], inferred from experiments [21–23], or obtained from first-principles calculations [24,25]. Studies of such models usually rely on one of two standard approaches. The first is to perform kinetic Monte Carlo (KMC) simulations, which yield a description of morphological evolution that is amenable to direct comparison with experiments [21–23,26–28]. In the second approach, a continuum theory is advanced as a coarse-grained, but computationally more efficient, description of the underlying atomistic dynamics. In the case of homoepitaxial growth, symmetry considerations and dynamic scaling have allowed the systematic classification of lattice models into universality classes corresponding to asymptotic continuum equations [10]. This represents the ultimate reduction of different growth scenarios to their most basic elements.

Homoepitaxial growth results from fundamental atomistic processes that are also operative for other growth scenarios [8], and, hence, provides a "laboratory" for studying the basic steps of the more complex processes during metallorganic vapor-phase epitaxy (MOVPE) and heteroepitaxial growth. Thus, homoepitaxial growth is often used to establish relationships between atomistic processes and their morphological manifestations [8,10,19] unencumbered by the gas-phase reactive environment of MOVPE or the nonlocal interactions present in heteroepitaxial systems. Moreover, in many technological applications, smooth and abrupt homoepitaxial interfaces are critical factors for determining device performance [29–33]. This endows homoepitaxial growth with a technological importance in its own right.

From a theoretical perspective, establishing direct relationships between atomistic processes and continuum equations governing homoepitaxial morphologies is especially important. In practice, however, it is difficult [31–33] to quantitatively relate continuum equations to observed morphologies because the coefficients in such equations [34–43] are, in effect, arbitrary. Moreover, experiments and computer simulations only access transient regimes of morphological evolution, whereas universality, which is often invoked [10,11] to justify a particular continuum equation for a given experimental setup, is appropriate only in the limit of infinitely large length and time scales. Indeed, the difficulties encountered with the description of recent computer simulations [45–47] and experiments [30–33,48–50] of homoepitaxial growth in terms of the standard equations of surface growth show that this program remains problematic. This is exacerbated by the fact that, from a technological perspective [29–33], the initial rather than the asymptotic behavior of homoepitaxial surfaces, is of primary interest.

The purpose of the present paper is to systematically derive continuum equations from generic atomistic processes of homoepitaxial growth for any length and time scales. We will use a previously developed [51–53] general approach for the renormalization of lattice models that is described in detail in a companion paper [54]. Lattice Langevin equations are first obtained from Chapman-Kolmogorov equations governing the lattice dynamics [55,56]. These equations embody the statistical properties of lattice models and are suitable for direct analysis, as well as providing a computational alternative to KMC simulations. For our purposes, the lattice Langevin formulation constitutes a starting point for coarse-graining in that the associated continuum equations serve as initial conditions for a dynamic renormalization-group (RG) analysis, which produces the correct continuum description for any length and time scales. The parameters in the continuum descriptions take numerical values that are determined directly by the underlying atomistic kinetics. Our RG analysis is general enough to allow the determination of a hierarchy of coarse-grained expressions for most lattice models of homoepitaxial growth, which opens the way to analytic studies of transient regimes observed during homoepitaxy.

The method outlined above will be implemented for an atomistic realization of the Edwards-Wilkinson (EW) model, the Wolf-Villain (WV) model, and a basic model for thermally activated surface diffusion. The lattice formulation of the EW model [36,57] is often employed as a prototype model in the statistical mechanics community [10,46,57–59], and we will use this model in a similar way to illustrate our multiscale approach for a particularly simple case. A more challenging application is the WV model [60], which was originally proposed [61] as the mechanism for low-temperature homoepitaxy of group-IV materials. For one-dimensional (1D) substrates our analysis [51,54] has been shown to reproduce the crossover sequence known from KMC simulations [44,56,60,62], with a kinetically rough surface morphology described asymptotically by the EW equation. For two-dimensional (2D) substrates, however, we find a transition from smooth to unstable morphologies characterized by self-organized mounds. This offers a qualitative explanation of recent growth experiments on Ge(001) [30] with the intriguing conclusion that the mechanism responsible for ordered films in the early stages of growth leads to an instability at longer times. For high enough temperatures activated surface diffusion delays this instability, but eventually the surface becomes unstable even if surface diffusion strongly dominates over WV relaxation processes at atomistic scales. Indeed, our results provide an analytic justification for the conclusion reached by KMC simulations [44–46] that a given relaxation mechanism can lead to qualitatively different surface morphologies depending on the dimensionality of the substrate (i.e., nonuniversal behavior) and the length and time scales considered.

Concurrent random deposition and thermally activated surface diffusion provides the standard basic lattice model for epitaxial growth [26–28]. Simulations of this model [44,63] reveal a surprisingly complex crossover sequence which strongly depends on the numerical values of model parameters such as the nearest-neighbor binding energy and the substrate temperature. In all cases, the asymptotic scaling behavior corresponds to the equation proposed by Villain [40] and by Lai and Das Sarma [41]. The RG trajectories calculated for this model reproduce all of the results obtained from KMC simulations [52], but with the added advantage that the equations at any point along the RG trajectories are related directly to the transition rates of the original lattice model. Our method can therefore be used to analyze experimental data, which corresponds to the transient regimes of the RG trajectories, and not just the asymptotic regimes.

The organization of this paper is as follows. Section II reviews the basic elements of our method [51–54] for the multiscale analysis of stochastic lattice models. In Secs. III–V we describe the application of this method to the EW and WV models and to thermally activated surface diffusion. For all three models, we calculate the corresponding RG trajectories, which we compare with results obtained from KMC simulations and, for the WV model, with the experiments on Ge(001) noted above. In Sec. VI we show how the RG transformations of the WV model and surface diffusion can be combined to obtain, in a rather straightforward manner, a multiscale theory of a prototypical model of homoepitaxial growth. Section VII contains a discussion of the application of our method to other growth scenarios and to other types of stochastic lattice models. A summary and conclusions are provided in Sec. VIII.

II. GENERAL METHOD

This section outlines the basic principles of our method [51–53] for the renormalization of stochastic lattice models. A more detailed formulation of this approach can be found in a companion paper [54], which focuses on 1D substrates ($d=1$). The changes in the formulation of our method necessitated by 2D substrates ($d=2$) are of a purely formal nature, though, for some models, 2D substrates can introduce several substantial technical issues. These will be addressed as the need arises.

Our starting point is the formulation of Markovian lattice models in terms of Chapman-Kolmogorov and master equations, which are then transformed into lattice Langevin equations (Sec. II A). Lattice Langevin equations embody the full atomistic transition rules and can be regularized to obtain continuum Langevin equations (Sec. II B). The coefficients in the continuum equations are determined directly by the atomistic kinetics and reflect the microscopic properties of the system under consideration. Section II C describes how the basic equation for homoepitaxial growth obtained for the models studied in this paper can be coarse-grained using RG methods.

A. Lattice Langevin equations

Molecular dynamics simulations of MBE demonstrate [64–66] that atomic trajectories for adatom hopping resemble irregular orbits located close to lattice sites, which only occasionally take an atom from one site to another. This observation motivates the description of MBE in terms of lattice models, in which each vibrational cycle of an adatom bound to a given lattice site is viewed as an attempt to escape from the local potential well associated with that site [19,20,66]. To account for the fact that many attempts are required before the adatom escapes, the vibrational frequency is multiplied by a factor that represents the probability per attempt for an escape. Thus, the effect of fast dynamical events is taken into account by stochastic transition rates for slower events [20].

In this paper we are concerned with stochastic lattice models which are completely characterized by an array $\mathbf{H}=\{H_{1,1},H_{1,2},\ldots,H_{L,L}\}$ for a 2D lattice of size $L\times L$, with similar notation for surfaces of other dimensions. For simplicity we take the lattice to have cubic symmetry, but all the following considerations can be extended to other lattice symmetries. In all the models considered here we impose the solid-on-solid criterion [67], wherein vacancies and overhangs are forbidden, so every atom has an atom beneath it. Thus, H_{ij} represents the height of the column of atoms at site (i,j).

The transition rates of such lattice models depend only on the instantaneous surface profile, not on its history. Systems that satisfy this condition are referred to as "Markovian" and are used to model a great variety of physical phenomena [68]. In particular, experiments [21–23,69] and *ab initio* calculations [24,66] suggest that the basic processes of surface growth can be approximated by Markovian lattice dynamics [70]. The morphological evolution of growing surfaces is then modeled by a set of atomistic processes that cause the heights $\mathbf{H}$ to change by integer multiples of the perpendicular lattice spacing at discrete times.

In mathematical terms, stochastic lattice models are defined by the Chapman-Kolmogorov equation [68] for the transition probability $T_{t+t'}(\mathbf{H}_3|\mathbf{H}_1)$ from height configuration $\mathbf{H}_1$ to configuration $\mathbf{H}_3$ in the time interval $t+t'$,

$$T_{t+t'}(\mathbf{H}_3|\mathbf{H}_1)=\sum_{\mathbf{H}_2}T_{t'}(\mathbf{H}_3|\mathbf{H}_2)T_t(\mathbf{H}_2|\mathbf{H}_1), \tag{1}$$

where $t=t_2-t_1$ and $t'=t_3-t_2$. The differential form of this equation, expressed in terms of the small-time limit of the transition probability, is the master equation [68],

$$\frac{\partial P}{\partial t}=\sum_{\mathbf{r}}[W(\mathbf{H}-\mathbf{r};\mathbf{r})P(\mathbf{H}-\mathbf{r},t)-W(\mathbf{H};\mathbf{r})P(\mathbf{H},t)], \tag{2}$$

where $P(\mathbf{H},t)\equiv T_t(\mathbf{H}|\mathbf{H}_1)$, $W(\mathbf{H};\mathbf{r})$ is the transition rate from $\mathbf{H}$ to $\mathbf{H}+\mathbf{r}$, and $\mathbf{r}=\{r_{1,1},r_{1,2},\ldots,r_{L,L}\}$ is the array of jump lengths between height configurations.

As an example, consider the transition rate for the hopping of a single particle from a site (i,j) to a site (k,l):

$$W_1(\mathbf{H};\mathbf{r})=\sum_{i,j;k,l}w_{i,j;k,l}\delta_{r_{i,j},-a_\perp}\delta_{r_{k,l},a_\perp}\prod_{\substack{m\neq i,k\\ n\neq j,l}}\delta_{r_{m,n},0}, \tag{3}$$

where $\delta_{m,n}$ is the Kronecker delta and $a_\perp$ is the perpendicular lattice spacing. The hopping rate and hopping rules are contained in the $w_{i,j;k,l}$, which can depend only on the initial configuration of the active adatom, as for many models of surface diffusion [55], the final configuration only, as for hopping with exclusion [71], or on both the initial and final configurations, as for hopping near step-edge barriers [72] and Metropolis implementations of hopping [73]. A common model for surface diffusion is nearest-neighbor hopping with Arrhenius [70] rates whose energy barrier $E_{i,j}$ is calculated from the initial environment of the active atom. In this case we have

$$w_{i,j;k,l} = \tfrac{1}{4}\nu_0 e^{-\beta E_{i,j}}(\delta_{i,k-1}\delta_{j,l} + \delta_{i,k}\delta_{j,l-1} + \delta_{i,k+1}\delta_{j,l} + \delta_{i,k}\delta_{j,l+1}), \tag{4}$$

where the attempt frequency $\nu_0 \approx 10^{12}-10^{13}$ s^{-1} [70] subsumes fast dynamical events and $\beta=(k_BT)^{-1}$, in which k_B is Boltzmann's constant and T is the absolute temperature of the substrate. With the above model, atoms hop from the top of the initial column to the top of the target column, a process that is usually referred to as "height diffusion." In particular, no account is taken of the height difference between columns, which amounts to infinite vertical diffusion. This unphysical effect is expected to be important only in regimes where the surface roughness admits large height differences between neighboring columns.

The master equation (2) can be transformed [53–56] into a more tractable form on the basis of the Kramers-Moyal-van Kampen expansion [68] and implementations of limit theorems due to Kurtz [74–82] to obtain a Fokker-Planck equation that embodies the statistical properties of the master and Chapman-Kolmogorov equations. The Fokker-Planck and its associated Langevin equation are formulated in terms of continuous height and time variables which necessitates the extension [53,54,56] of the rules of the original (discrete) transition rules to continuous height and time variables. Thus, one obtains [53–56] the lattice Langevin equation

$$\frac{dh_{i,j}}{d\tau} = K_{i,j}^{(1)} + \eta_{i,j}, \tag{5}$$

for $i=1,2,\ldots,L$ and $j=1,2,\ldots,L$, where $h_{i,j}$ and τ are continuous height and time variables, $K_{i,j}^{(1)}$ is the first moment of the transition rate density, and the $\eta_{i,j}$ are Gaussian noises that have zero mean and covariances

$$\langle \eta_{i,j}(\tau)\eta_{k,l}(\tau')\rangle = K_{i,j;k,l}^{(2)}\delta(\tau-\tau'), \tag{6}$$

in which $K_{i,j;k,l}^{(2)}$ is the second moment of the transition rate density and $\delta(x)$ is the Dirac delta function. The transition moments are defined by

$$K_{i,j}^{(1)}(\mathbf{h}) = \int r_{i,j}W(\mathbf{h};\mathbf{r})d\mathbf{r}, \tag{7}$$

$$K_{i,j;k,l}^{(2)}(\mathbf{h}) = \int r_{i,j}r_{k,l}W(\mathbf{h};\mathbf{r})d\mathbf{r}. \tag{8}$$

The form of the transition rate density $W(\mathbf{h};\mathbf{r})$ is identical to $W(\mathbf{H};\mathbf{r})$ in Eq. (2) for integer height configurations, and can be identified from physical considerations [53,54,56,71,78–80] for noninteger values of $\mathbf{h}$ and $\mathbf{r}$.

Returning to our example of random hopping, one finds [53] that the substitution of Eq. (3) with Eq. (4) into Eqs. (7) and (8) gives

$$K_{i,j}^{(1)} = \tfrac{1}{4}a_\perp\Delta^2\lambda_{i,j}, \tag{9}$$

$$K_{i,j;k,l}^{(2)} = \tfrac{1}{4}a_\perp^2[\delta_{i,k}\delta_{j,l}\Delta^2\lambda_{i,j} - \lambda_{i,j}\Delta^2(\delta_{i,k}\delta_{j,l}) - \Delta^2(\lambda_{i,j}\delta_{i,k}\delta_{j,l})], \tag{10}$$

where $\lambda_{i,j}=\nu_0 e^{-\beta E_{i,j}}$, and the discrete second difference

$$\Delta^2 f_{i,j} = f_{i-1,j} + f_{i,j-1} + f_{i+1,j} + f_{i,j+1} - 4f_{i,j} \tag{11}$$

acts only on the indices (i,j) in Eq. (10). The extension of the rules of random hopping to continuous variables amounts [53,56] to the interpolation of $E_{i,j}=E_{i,j}(\mathbf{h})$.

Lattice models for surface growth typically have threshold character and, as a result, the transition rate in Eq. (2) often involves the discrete step function θ_d:

$$\theta_d(\Delta H) = \begin{cases} 1 & \text{if } \Delta H \geq 0, \\ 0 & \text{if } \Delta H < 0, \end{cases} \tag{12}$$

for *discrete* height differences ΔH. The extension of the growth rules to continuous height variables necessitates expressing θ_d in terms of a continuous function. A convenient representation is [53,54]

$$\theta(\Delta h;\delta) = \frac{1}{2a}\int_{-\infty}^{a_\perp^{-1}\Delta h}\{\mathrm{erf}[(s+a)\delta] - \mathrm{erf}(s\delta)\}ds, \tag{13}$$

where $\mathrm{erf}(x)$ is the error function, $0<a\leq 1$, and $\delta>0$. The value of a depends on the rules of the model under consideration and must be chosen such that, for $\lim_{\delta\to\infty}\theta(\Delta H;\delta) = \theta_d(\Delta H)$, the transition rules of the original model are extended to continuous height and time variables. Where such values of a have been identified [54–56,84], the lattice Langevin formulation reproduces key properties of the original lattice model [53,54,56,71,78–80,83,84]. Despite its "atomic resolution," Eq. (5) is simple enough to allow a direct mathematical analysis and serves as the basis for the regularization of lattice models. This is discussed in the next section.

B. Continuum Langevin equations

The lattice Langevin equation (5) can be regularized to obtain a *continuum* equation by first introducing the continuous space variables (x_1,x_2) and the analytic height function $u(x_1,x_2,\tau)$, which has the Taylor expansion

$$h(i\pm n, j\pm m, \tau) = \sum_{k,l=0}^{\infty}\left(\frac{\partial^{k+l}u}{\partial x_1^k\,\partial x_2^l}\right)\Bigg|_{(i,j)}\frac{(\pm a_\parallel n)^k}{k!}\frac{(\pm a_\parallel m)^l}{l!}, \tag{14}$$

where $a_\parallel$ is the lateral lattice spacing. The transition moments of the lattice models considered in this paper involve nonanalytic step functions, which we regularize according to Eq. (13). For finite δ the expansion

$$\theta(\Delta h;\delta) = A(\delta;a) + \frac{B(\delta;a)}{a_\perp}\Delta h + \frac{C(\delta;a)}{a_\perp^2}(\Delta h)^2 + \cdots \tag{15}$$

has an infinite radius of convergence.

Upon substitution of Eqs. (14) and (15) into Eq. (5) one obtains a continuum equation with a convergent series of successively higher spatial derivatives. For large δ this produces [53,54] an essentially exact continuum version of Eq. (5). Decreasing δ amounts to a smoothing of height configurations and leads to an effective lower-order equation. For

some $\delta < \delta'$ the lowest-order equation [53,54] that embodies fundamental properties of the lattice model such as scaling behavior is obtained. This is the leading-order equation for the lattice model under consideration and our starting point for coarse-graining.

1. Continuum formulation of drift

Using the expansions in Eqs. (14) and (15) one finds that the deterministic drift in stochastic growth models takes the general form

$$K^{(1)}(\mathbf{x}) = f(\delta) + g[u, (\nabla u)^2, \ldots, \nabla^2 u, \ldots], \tag{16}$$

where $\mathbf{x}=(x_1,x_2)$. The arguments of g are expected to include all terms that are consistent with the symmetry of the lattice model [10], which serves as an independent check of this representation. The function f, on the other hand, corresponds to a constant growth rate of the surface, and can often be absorbed into a redefinition of the time in the continuum Langevin equation. Clearly f only has physical significance if it is independent of the value of δ. Indeed, one finds [53,84,85] $f=f(\delta)$ only for models of nonconserved and amorphous growth, for which the growth rate depends on the height configuration and is not a generic property of the growth process.

In the case of epitaxial growth without desorption, for which the material deposited is equal to the sum (or integral) over the surface height at any time, one finds that the general expression in Eq. (16) reduces to

$$K^{(1)}(\mathbf{x}) = F + \nabla \cdot \mathbf{J}(u, \nabla u, \ldots), \tag{17}$$

where $F=a_\perp/\tau_0$ is the deposition flux, in which $1/\tau_0$ is the deposition rate. The first term in this expression corresponds to the constant deposition flux. The second term describes the deterministic part of the evolution of the fluctuating surface, which for conserved growth models such as Eq. (9) can be written as the divergence of a current $\mathbf{J}$. Thus, the deterministic part of the dynamics takes the form of a conservation law [10].

2. Continuum formulation of diffusion

For lattice models that combine deposition with instantaneous relaxation [10], the second moment in Eq. (8) is diagonal with the elements of the first moment as its entries [55,56,86]. For such models, which will be discussed in Secs. III and IV, the continuum limit of the diffusion term in the lattice Langevin equation is trivial, once appropriate expressions for the first moments have been identified. In general, however, the second moment contains off-diagonal elements and the continuum limit of the diffusion term is more complicated. This can be illustrated for the model for random hopping introduced in Sec. II A. We have

$$\lambda_{i,j} \to \lambda(\mathbf{x}),$$

$$\delta_{i,k}\delta_{j,l} \to a_\parallel^2 \delta^2(\mathbf{x}-\mathbf{x}'),$$

$$\Delta^2 \to \frac{2}{2!}a_\parallel^2\left(\frac{\partial^2}{\partial x_1^2}+\frac{\partial^2}{\partial x_2^2}\right)+\frac{2}{4!}a_\parallel^4\left(\frac{\partial^4}{\partial x_1^4}+\frac{\partial^4}{\partial x_2^4}\right)+\cdots, \tag{18}$$

where the continuum limit of λ in Eqs. (9) and (10) is taken according to Eqs. (14) and (15). Thus keeping terms of second order only, the continuum limit of the covariance in Eq. (10) is [53]

$$K^{(2)}(\mathbf{x},\mathbf{x}') = \tfrac{1}{4}a_\perp^2[-2\nabla\cdot\{\lambda(\mathbf{x})\nabla[a_\parallel^2\delta^2(\mathbf{x}-\mathbf{x}')]\}]. \tag{19}$$

Higher-order corrections to Eq. (19) can also be written as the divergence of a current [53], implying that the noise is conserved [10,53].

3. Continuum formulation of homoepitaxial growth

For the prototypical atomistic processes of homoepitaxial growth considered in this paper, the continuum limit of the drift and diffusion terms in the lattice Langevin equation (5) yields

$$\frac{\partial u}{\partial \tau} = \nu_2\nabla^2 u - \nu_4\nabla^4 u + \lambda_{13}\nabla(\nabla u)^3 + \lambda_{22}\nabla^2(\nabla u)^2 + F + \xi, \tag{20}$$

where $\nabla(\nabla u)^3 \equiv \nabla\cdot[(\nabla u)^2\nabla u]$ and the smoothed Gaussian noise $\xi(\mathbf{x},\tau)$ has zero mean and covariance

$$\langle \xi(\mathbf{x},\tau)\xi(\mathbf{x}',\tau')\rangle = 2\mathcal{D}\delta(\mathbf{x}-\mathbf{x}')\delta(\tau-\tau'), \tag{21}$$

in which $\mathcal{D}=D_0-D_2\nabla^2$, where $D_0=a_\parallel^d a_\perp F/2$ and D_2 are constants associated with the strength of nonconserved and conserved fluctuations. The signs and magnitudes of the coefficients in Eq. (20) depend on the lattice model under consideration. The stability of linear perturbations requires that $\nu_2>0$ and $\nu_4>0$. Special cases of Eq. (20) have been extensively studied as asymptotic descriptions of homoepitaxial growth [10,34,35,39–42], but the derivation of this equation directly from lattice transition rules means that both transient and asymptotic regimes can be examined in detail.

C. Renormalized Langevin equations

The continuum limit of the lattice Langevin equation (5) provides the starting point for the systematic coarse-graining of lattice models [51–54]. The RG trajectory of the model is obtained by solving the RG equations for the microscopic Langevin equation with the coefficients obtained from the atomistic kinetics as initial conditions. Successive RG transformations "weed out" terms in the continuum equation that become irrelevant at larger scales and absorb their effect into the remaining terms. This procedure provides a "minimal" continuum representation of the atomistic kinetics in which only features operating at that particular scale are retained.

1. Renormalization group equations

The RG analysis of the leading-order Langevin equation for homoepitaxy (20) is developed in Refs. [53,54] and the result is summarized here for completeness. Consistent with previous studies [10,42] we find that under the RG the noise

covariance in Eq. (21) is modified to $\mathcal{D}=D_0-D_2\nabla^2+D_4\nabla^4$. The coefficients in Eq. (20) then renormalize under the change of scale $\mathbf{x}\to e^{d\ell}\mathbf{x}$, $\tau\to e^{zd\ell}\tau$, and $u\to e^{\alpha d\ell}u$ to one-loop order as [51,54]

$$\frac{d\nu_2}{d\ell}=(z-2)\nu_2+K_d\frac{d+2}{d}\frac{\lambda_{13}D\Lambda^d}{\nu}, \tag{22}$$

$$\frac{d\nu_4}{d\ell}=(z-4)\nu_4-\frac{K_d}{d}\frac{\lambda_{22}^2D_s\Lambda^d}{\nu^3}, \tag{23}$$

$$\frac{d\lambda_{13}}{d\ell}=(z-4+2\alpha)\lambda_{13}-\frac{AK_d}{d(d+2)}\frac{\lambda_{13}^2D\Lambda^d}{\nu^2}, \tag{24}$$

$$\frac{d\lambda_{22}}{d\ell}=(z-4+\alpha)\lambda_{22}-2K_d\frac{d+2}{d}\frac{\lambda_{13}\lambda_{22}D\Lambda^d}{\nu^2}, \tag{25}$$

$$\frac{dD_0}{d\ell}=(z-d-2\alpha)D_0, \tag{26}$$

$$\frac{dD_2}{d\ell}=(z-d-2\alpha-2)D_2, \tag{27}$$

$$\frac{dD_4}{d\ell}=(z-d-2\alpha-4)D_4+K_d\frac{\lambda_{22}^2D^2\Lambda^{d-2}}{\nu^3}, \tag{28}$$

where $K_d=S_d/(2\pi)^d$, $S_d=2\pi^{d/2}/\Gamma(\frac{1}{2}d)$ is the surface area of a d-dimensional unit sphere, Λ is the momentum cutoff, and

$$A=d^2+6d+20, \tag{29}$$

$$\nu=\nu_2+\nu_4\Lambda^2, \tag{30}$$

$$D=D_0+D_2\Lambda^2+D_4\Lambda^4, \tag{31}$$

$$D_s=\sum_{i=0}^{2}[(d-4+2i)\nu-2\nu_4\Lambda^2]D_{2i}\Lambda^{2i}. \tag{32}$$

The flow parameter ℓ in Eqs. (22)–(28) describes the degree of coarse-graining between microscopic ($\ell=0$) and macroscopic ($\ell\to\infty$) regimes.

The scaling exponents z and α take constant numerical values at fixed points of the RG, but vary during crossover regimes. The full RG trajectories of atomistic models of homoepitaxial growth can be calculated by introducing the dimensionless quantities

$$r=\frac{\nu_4\Lambda^2}{\nu_2+\nu_4\Lambda^2}, \tag{33}$$

$$u_1=K_d\frac{3d^2+14d+28}{d^2(d+2)}\frac{D_0\lambda_{13}\Lambda^d}{(\nu_2+\nu_4\Lambda^2)^2}, \tag{34}$$

$$u_2=\left[K_d\frac{3(6-d)}{d(4-d)}\frac{D_0\lambda_{22}^2\Lambda^{d+2}}{(\nu_2+\nu_4\Lambda^2)^3}\right]^{1/2}, \tag{35}$$

$$\Gamma_2=\frac{D_2\Lambda^2}{D_0}, \tag{36}$$

$$\Gamma_4=\frac{D_4\Lambda^4}{D_0}, \tag{37}$$

in terms of which the RG equations (22)–(28) do not directly involve the scaling exponents [53,54]:

$$\frac{dr}{d\ell}=-2r(1-r)-2Bru_1\Gamma+2C(1-r)u_2^2\Gamma_s, \tag{38}$$

$$\frac{du_1}{d\ell}=u_1(-d+4r-du_1\Gamma-4Cu_2^2\Gamma_s), \tag{39}$$

$$\frac{du_2}{d\ell}=u_2\left[-\tfrac{1}{2}(d+2)+3r-7Bu_1\Gamma-3Cu_2^2\Gamma_s\right], \tag{40}$$

$$\frac{d\Gamma_2}{d\ell}=-2\Gamma_2, \tag{41}$$

$$\frac{d\Gamma_4}{d\ell}=-4\Gamma_4+2dCu_2^2\Gamma^2, \tag{42}$$

where we have used the scaling relation implied by Eq. (26) [10,41,42,53], $\Gamma=1+\Gamma_2+\Gamma_4$,

$$\Gamma_s=4-d+2r+\Gamma_2(2-d+2r)+\Gamma_4(-d+2r), \tag{43}$$

and

$$B=\frac{d(d+2)^2}{2(3d^2+14d+28)},$$

$$C=\frac{4-d}{6(6-d)}. \tag{44}$$

The solution of Eqs. (38)–(42) with the microscopic Eq. (20) as the initial condition amounts to the renormalization of the original stochastic lattice model.

2. Fixed points

The transformed RG equations (38)–(42) are simple enough to allow a general solution [53,54] for all possible fixed points associated with Eq. (20). The Langevin equations corresponding to these fixed points are the stable macroscopic limits of the microscopic Langevin equation (20). The fixed-point Langevin equations which are most relevant for the models studied in this paper are the EW equation [36],

$$\frac{\partial u}{\partial\tau}=\nu_2\nabla^2u+\xi, \tag{45}$$

the Mullins-Herring (MH) equation [34,35],

$$\frac{\partial u}{\partial\tau}=-\nu_4\nabla^4u+\xi, \tag{46}$$

and the Villain-Lai-Das Sarma (VLDS) equation [40,41],

$$\frac{\partial u}{\partial \tau} = -\nu_4 \nabla^4 u + \lambda_{22} \nabla^2 (\nabla u)^2 + \xi. \tag{47}$$

We have removed the constant deposition flux F in each equation by transforming $u \to u + F\tau$, so that u describes the fluctuations about the average height.

For a nonzero deposition flux, the Gaussian noise ξ in the fixed-point Langevin equations (45)–(47) has zero mean and the covariance in Eq. (21) with $D_2=0$ [54]. For the EW and MH fixed points we also have $D_4=0$, whereas $D_4 \neq 0$ at the VLDS fixed point [42,54]. Variations of Eqs. (46) and (47) are the *conserved* MH (cMH) equation [10] and the *conserved* VLDS (cVLDS) equation [39], for which $D_0=0$ and $D_2 \neq 0$. The RG equations (22)–(28) imply that no fixed point with $D_2 \neq 0$ can be obtained asymptotically for a nonzero deposition flux, but conserved fluctuations can nevertheless determine extended transient regimes [51–53,87,88].

III. EDWARDS-WILKINSON MODEL

The EW equation (45) was proposed initially [36] for the sedimentation of particle aggregates following vertical trajectories. The discrete version of this theory, which we call the EW model, was formulated [57] for surfaces driven by random deposition, but with limited diffusion. A number of different incarnations of the EW model [46,57–59] have been investigated with KMC simulations. In the version we study here, a particle deposited onto a randomly chosen lattice site remains at that site only if its height is less than or equal to the heights at all nearest-neighbor sites. Otherwise, the final deposition site is chosen randomly from nearest-neighbor sites with lower heights. We will use this model to illustrate some of the technical issues connected with the derivation of transition moments for lattice models combining random deposition with instantaneous relaxation.

A. Analytic formulation

The formulation of the lattice Langevin equation for the EW model necessitates the calculation of the first and second moments of the transition rate density in Eqs. (7) and (8). For models such as the EW model which combine deposition with instantaneous relaxation, the second moment can be expressed in terms of the first moment:

$$K^{(1)}_{i,j} = a_\perp [w^{(1)}_{i,j} + w^{(2)}_{i+1,j} + w^{(3)}_{i,j+1} + w^{(4)}_{i-1,j} + w^{(5)}_{i,j-1}], \tag{48}$$

$$K^{(2)}_{i,j;k,l} = a_\perp K^{(1)}_{i,j} \delta_{i,k} \delta_{j,l}, \tag{49}$$

where $w^{(n)}_{i,j}$ is the local transition rate for a particle deposited at site (i,j) to remain there $(n=1)$, to hop to site $(i \mp 1, j)$ $(n=2,4)$, or to site $(i, j \mp 1)$ $(n=3,5)$. The generalization of Eqs. (48) and (49) to models that allow relaxation to more distant sites is straightforward. The key point is that, for transition rates that induce only constant changes in the occupancy of single sites, all higher-order transition moments are diagonal with entries equal to the first moment.

The local transition rates are composed of all height configurations resolved by the rules of the lattice model. For the EW model, these are generated by expanding the identity

$$f(H_{i+1,j} - H_{i,j}) f(H_{i-1,j} - H_{i,j}) f(H_{i,j+1} - H_{i,j}) f(H_{i,j-1} - H_{i,j}) = 1, \tag{50}$$

where we have defined

$$f(\Delta H) = \Theta_d(\Delta H) + \theta_d(\Delta H), \tag{51}$$

with

$$\Theta_d(\Delta H) = 1 - \theta_d(\Delta H), \tag{52}$$

in which $\theta_d(\Delta H)$ is the discrete step function defined in Eq. (12).

Equation (50) produces $2^4=16$ distinct height configurations, which are allocated to the local transition rates in Eq. (48) according to the rules of the EW model:

$$w^{(1)}_{i,j} = \theta_{-i} \theta_i \theta_{-j} \theta_j, \tag{53}$$

$$\begin{aligned} w^{(2)}_{i,j} = {} & \theta_i \theta_{-j} \theta_j \Theta_{-i} + \tfrac{1}{2} \theta_{-j} \theta_j \Theta_{-i} \Theta_i + \tfrac{1}{2} \theta_i \theta_j \Theta_{-i} \Theta_{-j} + \tfrac{1}{2} \theta_i \theta_{-j} \Theta_{-i} \Theta_j \\ & + \tfrac{1}{3} \theta_{-j} \Theta_{-i} \Theta_i \Theta_j + \tfrac{1}{3} \theta_j \Theta_{-i} \Theta_i \Theta_{-j} + \tfrac{1}{3} \theta_i \Theta_{-i} \Theta_{-j} \Theta_j \\ & + \tfrac{1}{4} \Theta_{-i} \Theta_i \Theta_{-j} \Theta_j, \end{aligned} \tag{54}$$

in which we use the notation $\theta_{\pm i} \equiv \theta_d(H_{i\pm1,j} - H_{i,j})$ and $\theta_{\pm j} \equiv \theta_d(H_{i,j\pm1} - H_{i,j})$, with analogous definitions for $\Theta_{\pm i}$ and $\Theta_{\pm j}$, and we have set $\tau_0=1$. The remaining transition rates, $w^{(3)}_{i,j}$, $w^{(4)}_{i,j}$, and $w^{(5)}_{i,j}$, are obtained from $w^{(2)}_{i,j}$ by anticlockwise rotations about the central point (i,j) through angles of $\frac{1}{2}\pi$, π, and $\frac{3}{2}\pi$ rad, respectively. Since the transition rules of the EW model conserve the number of particles, the local transition rates must satisfy

$$\sum_{k=1}^{5} w^{(k)}_{i,j} = 1, \tag{55}$$

which serves as a check of the expressions for the local transition rates. Our construction of the local transition rates from Eq. (50) ensures that this sum rule is satisfied.

Expressions for the first and second moments appropriate for the continuous height and time variables $\mathbf{h}$ and τ in the lattice Langevin equation (5) are obtained by generalizing the rules of the lattice model to continuous variables [53,54,56]. For the EW model this can be achieved by replacing θ_d with $\theta(\Delta h; \delta)$ defined in Eq. (13). We find [53,56] that Eq. (13) with $a \to 0$ provides, for $\delta \to \infty$, a suitable generalization of the rules of the EW model to continuous variables. This is confirmed [53,56] by comparing the results of KMC simulations with those obtained from the integration of Eq. (5).

Equations (50) and (53)–(55) are readily generalized to substrates of any dimensions. In d substrate dimensions the identity in Eq. (50) generates 2^{2d} configurations, so our procedure can be applied for higher substrate dimensions without undue computational effort. For more complex lattice models with rules that resolve a large number of height configurations similar considerations can be used to construct algorithms for the computation of transition moments. This will be discussed further in Sec. IV.

B. Continuum Langevin equation

The expressions for the first and second moments in Eqs. (48) and (49), together with Eqs. (53) and (54) and the prescription $a \to 0$ in Eq. (13), completely specify the lattice Langevin equation (5) for the EW model. The corresponding continuum Langevin equation is obtained by introducing the continuous space variables (x_1, x_2) and the interpolating height function $u(x_1, x_2, \tau)$ according to Eq. (14), and expanding θ as in Eq. (15). Upon substitution of these expansions into Eqs. (5), (48), and (49) we obtain, for $\delta < \delta'$, the leading-order continuum Langevin equation associated with the EW model. From a practical perspective, the form of the leading-order equation and the numerical value of δ' is determined [53,54] by comparing the maximum magnitudes of the coefficients at different orders in the spatial derivatives.

We consider the 1D EW model first. Denoting the maximum magnitude of coefficients of terms of order n in the spatial derivatives of $u(x, \tau)$ by $\max[O(n)]$, one finds

$$\max[O(2)] \approx 5 \max[O(4)] \quad \text{for} \quad \delta \lessapprox 0.5,$$

$$\max[O(4)] \approx 9 \max[O(6)] \quad \text{for} \quad \delta \lessapprox 0.02,$$

$$\max[O(6)] \gtrapprox 10 \max[O(8)] \quad \text{for} \quad \delta \lessapprox 0.3,$$

$$\max[O(8)] \gtrapprox 10 \max[O(10)] \quad \text{for} \quad \delta \lessapprox 0.03.$$

For the 2D EW model, we find

$$\max[O(2)] \approx 5 \max[O(4)] \quad \text{for} \quad \delta \lessapprox 0.3,$$

$$\max[O(4)] \approx 10 \max[O(6)] \quad \text{for} \quad \delta \lessapprox 0.1.$$

These estimates suggest that a basic description of the 1D and 2D EW models is already provided by the terms of $O(2)$ in the continuum expressions for the transition moments in Eqs. (48) and (49). Upon making the transformation $u \to u + F\tau$ this yields the EW equation (45) with a smoothed Gaussian noise $\xi(\mathbf{x}, \tau)$ which has zero mean and the covariance in Eq. (21) with $D_2 = 0$. It is not surprising that the EW equation (45) is obtained as a basic description of the EW model, even at atomistic scales. Indeed, it is well-known [10,57] that even for relatively small system sizes KMC simulations of the EW model show scaling behavior consistent with Eq. (45). Moreover, the 1D EW equation has been derived previously [89] as an asymptotic description of the 1D EW model. But there is also evidence from KMC simulations [46,58,59] of discrepancies between the EW equation and simulations of the EW model. As will be discussed below, our approach can be used to investigate such issues.

A more complete description of the EW model at atomistic scales must incorporate the leading-order couplings:

$$\frac{\partial u}{\partial \tau} = \nu_2 \nabla^2 u - \nu_4 \nabla^4 u + \nu_6 \nabla^6 u + \lambda_{13} \boldsymbol{\nabla} (\boldsymbol{\nabla} u)^3 + \lambda_{22} \nabla^2 (\boldsymbol{\nabla} u)^2 + \xi, \tag{56}$$

where the noise ξ is defined in Eq. (21) with $D_2 = 0$. Since the underlying lattice model is formulated on a cubic lattice, the continuum Langevin equation for the 2D EW model exhibits square symmetry rather than full rotational symmetry. We have obtained the simplified form in Eq. (56) by combining terms of the same order of spatial derivatives and powers of u, and averaging over the coefficients of these terms. The numerical values of the coefficients in Eqs. (21), (45), and (56) appropriate for the EW model are obtained with $0 < \delta < \delta' \approx 0.02$ for 1D substrates, and with $0 < \delta < \delta' \approx 0.1$ for 2D substrates. Table I provides a summary of these values for the representative choice $\delta = 0.01$. We thereby include the term $\nu_6 \nabla^6 u$ in Eq. (56), despite its higher order and the small magnitude of ν_6 relative to ν_2 and ν_4, for reasons of stability.

TABLE I. Rounded numerical values of the coefficients in Eqs. (21), (45), and (56) for the EW model on substrates of dimension d obtained with the representative choice $\delta = 0.01$. We have set $a_\perp = a_\parallel = \tau_0 = 1$ and we have $D_2 = 0$ for $d = 1$ and $d = 2$.

d	ν_2	ν_4	ν_6	λ_{13}	λ_{22}	D_0
1	1×10^{-2}	-2×10^{-3}	3×10^{-4}	-4×10^{-7}	2×10^{-5}	$\frac{1}{2}$
2	7×10^{-3}	-1×10^{-3}	8×10^{-5}	-2×10^{-7}	6×10^{-6}	$\frac{1}{2}$

C. Renormalization-group trajectories

Table I shows that ν_2 has the largest magnitude, even at microscopic scales. The term $\nu_2 \nabla^2 u$ is also the most relevant term in the scaling sense [10,54]. One can therefore expect to obtain an elementary description of the EW model at all scales already on the basis of Eq. (45). But note that the EW equation does not couple different length and time scales through nonlinear terms. Thus, a simple scaling analysis replaces the RG calculation described in Sec. II C, and the scaling behavior of the EW model is found to be simply that of the EW fixed point [10,36]. On the other hand, a more complete description is provided by Eq. (56), which involves the couplings for the EW model. A more accurate multiscale analysis of the EW model therefore necessitates the inclusion of the term $\nu_6 \nabla^6 u$ in the calculation of the RG trajectories from the initial conditions in Table I [53]. As discussed below, there may be cases where such an approach is necessary, but we have not pursued this line of investigation here.

Taking a more phenomenological perspective, we note that the magnitudes of ν_4 and ν_6 in Table I are small compared to ν_2. We therefore simply omit the terms $\nu_4 \nabla^4 u$ and $\nu_6 \nabla^6 u$ altogether and include only the couplings $\lambda_{13} \boldsymbol{\nabla} (\nabla u)^3$ and $\lambda_{22} \nabla^2 (\boldsymbol{\nabla} u)^2$ as higher-order terms in Eq. (56). The corresponding solutions of the RG flow equations for the 1D and 2D EW model are shown in Figs. 1 and 2. Superimposed on the trajectories are points separated by a logarithmic scale $\Delta \ell = 1/5$, which gives a basic qualitative notion of the "speed" of the flow along a given RG trajectory [53,54]. These trajectories suggest that for both substrate dimensions the EW model approaches the asymptotically stable EW fixed point in Eq. (45) with no crossovers involving other fixed points. Variations of δ within the range $0 < \delta < \delta'$ do not alter this result. The trajectories in Figs. 1 and 2 are consistent with KMC simulations [10,56,57] of the formulation of the EW model used here. Note, however, that in approaching the EW fixed point the RG trajectories of the EW

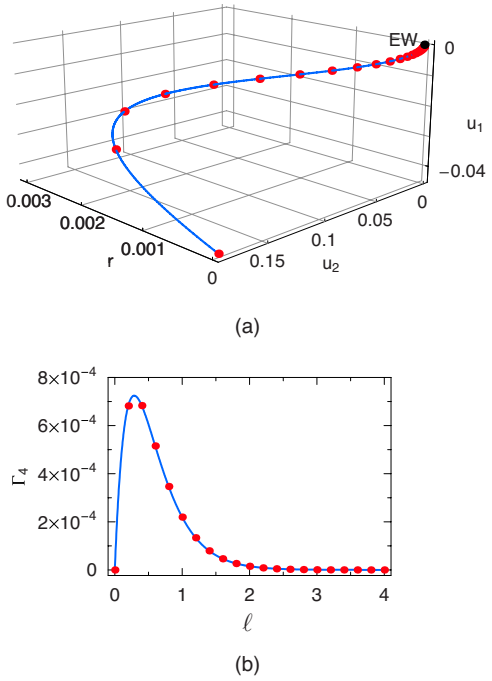

FIG. 1. (Color online) RG flow trajectory of the 1D EW model obtained from Eqs. (38)–(42) with the initial conditions in Table I with $\nu_4=\nu_6=0$: (a) RG flow of the deterministic part of Eq. (20) and (b) RG flow of the amplitude of fluctuations with $\Gamma_2=0$ at every point along the RG trajectory. After a transient regime the EW fixed point is approached asymptotically. The curves in panels (a) and (b) are obtained with $0\leq\ell\leq 4$. Superimposed on the RG trajectories are points separated by a logarithmic scale of $\Delta\ell=1/5$.

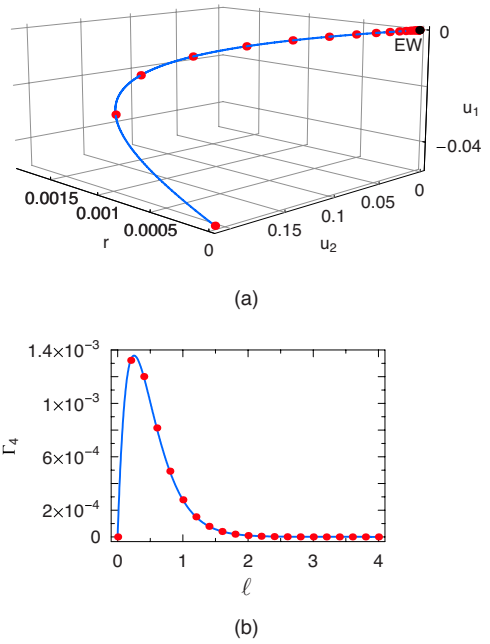

FIG. 2. (Color online) RG flow trajectory of the 2D EW model obtained from Eqs. (38)–(42) with the initial conditions in Table I with $\nu_4=\nu_6=0$: (a) RG flow of the deterministic part of Eq. (20) and (b) RG flow of the amplitude of fluctuations with $\Gamma_2=0$ at every point along the RG trajectory. After a transient regime the EW fixed point is approached asymptotically. The curves in panels (a) and (b) are obtained with $0\leq\ell\leq 4$. Superimposed on the RG trajectories are points separated by a logarithmic scale of $\Delta\ell=1/5$.

model change direction and, hence, the approach of the EW fixed point is nontrivial. This suggests that the transient behavior of the EW model is richer than a simple scaling analysis of the EW equation would suggest.

Large-scale computer simulations [46,58] of two modified versions of the EW model studied here have revealed anomalous scaling exponents for the 2D EW model that do not seem to conform to any known universality class. A possible mechanism for this behavior is provided by the negative sign of ν_4 in Eq. (56). If the term $\nu_6\nabla^6 u$, with $\nu_6>0$, is included in the continuum equation, the spectrum of linear perturbations $e^{i(\mathbf{k}\cdot\mathbf{r}+\omega t)}$ is

$$i\omega = -\nu_2 k^2 + |\nu_4| k^4 - \nu_6 k^6. \tag{57}$$

Thus, for $\nu_2 < \nu_4^2/(3\nu_6)$ there is an instability with the critical wave number

$$k_c = \left(\frac{|\nu_4|}{3\nu_6} + \frac{\sqrt{\nu_4^2 - 3\nu_2\nu_6}}{3\nu_6} \right)^{1/2}, \tag{58}$$

which produces a spatially periodic morphology. This would be manifested by a regime whose scaling exponents differ from the EW universality class.

The coefficient ν_2 and the noise covariance D_0 have recently [59] been measured from simulations of the EW model. The results suggest that in fact the two modified versions of the EW model studied in Refs. [46,58] belong to the EW universality class. In addition, the values of the coefficient ν_2 measured in Ref. [59] for the two modified versions of the EW model are essentially identical for 1D substrates. Including these modifications in the above derivation of the continuum equation, we indeed find that the coefficient ν_2 takes identical numerical values for these modified formulations of the EW model. On the other hand, in the case of 2D substrates the simulations suggest [59] that ν_2 takes smaller numerical values for transition rules that mandate that a deposited particle stays at the original deposition site if there is no unique nearest-neighbor site with minimum height. This is also found from our analysis. These results provide additional confirmation that Eq. (56) with the appropriate values for the coefficients obtained from the atomistic dynamics constitutes a suitable description of the EW model and its modifications. But a complete quantitative understanding of the results reported in Refs. [46,58,59] must await a more detailed RG analysis of Eq. (56).

IV. WOLF-VILLAIN MODEL

The WV model [60] was first proposed [61] as a mechanism for surface relaxation during the epitaxial growth of group-IV semiconductors at temperatures too low for activated surface diffusion. At such temperatures, ordered growth can still occur [90] because of short-range nonthermal motion of newly deposited species to increase their coordination [91,92]. Examples of this effect are transient mo-

bility [91–93], ballistic impact [94,95], and downward funneling [96]. The physical basis of the WV model [61] is that the condensation energy of deposited particles is dissipated by relaxation to a nearby site that maximizes its bonding coordination. The transition rules of the WV model [60,61] stipulate that a particle arriving at a randomly chosen site remains there only if its coordination cannot be increased by moving to a nearest-neighbor site. Otherwise, the final deposition site is chosen randomly from nearest-neighbor sites that offer the maximum coordination.

A. Analytic formulation

As for the EW model analyzed in Sec. III, the formulation of the lattice Langevin equation (5) associated with the WV model amounts to the calculation of expression (48) for the first moment of the transition rate density. For the 2D WV model all relevant height configurations are generated by the identity

$$\prod_{\mathcal{R}} \{f(H_{i+1,j} - H_{i+2,j}) f(H_{i+1,j} - H_{i+1,j-1}) \times f(H_{i+1,j} - H_{i+1,j+1}) g(H_{i,j} - H_{i+1,j})\} = 1, \quad (59)$$

where the product is to be taken over the sets of indices obtained through rotations by $\frac{1}{2}\pi$, π, and $\frac{3}{2}\pi$ rad about the site (i,j),

$$g(\Delta H) = \Theta_d(\Delta H) + \Theta_d(-\Delta H) + \delta(\Delta H), \quad (60)$$

with

$$\delta(\Delta H) = \theta_d(\Delta H) + \theta_d(-\Delta H) - 1, \quad (61)$$

and the functions θ_d, f, and Θ_d are defined in Eqs. (12), (51), and (52).

Equation (59) generates

$$(2 \times 2 \times 2 \times 3)^4 = 331\ 776 \quad (62)$$

distinct height configurations that must be allocated to the appropriate local transition rates in Eq. (48) according to the rules of the WV model. Owing to the complexity of the manipulations involved, the calculation of the local transition rates is most conveniently achieved using a symbolic computation program, such as MATHEMATICA [97], which we have used here. The algorithm is outlined in the Appendix and is formulated in analogy with the derivation of the transition moments for the EW model in Sec. III A. In the case of a 1D substrate only 36 distinct height configurations need to be considered and the corresponding lattice Langevin for the WV model has been derived elsewhere [56,98].

The structure of Eq. (59) leads to a subtlety in the analytic formulation of the WV model for substrate dimensions $d > 1$. To appreciate the problem, consider the sites (i,j), $(i+1,j)$, $(i+1,j-1)$, and $(i,j-1)$ in Fig. 3, which shows a plan view of the local height environment resolved by the 2D WV model. Equation (59) generates, for instance, a height configuration with

$$H_{i+1,j} > H_{i,j},$$

$$H_{i+1,j-1} > H_{i+1,j},$$

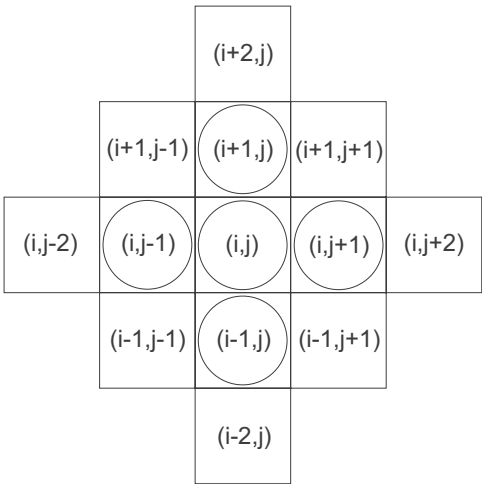

FIG. 3. Plan view of the local environment relevant for the 2D WV model. The initial deposition site is (i,j), and any of the sites marked with a circle may be selected as the final deposition site.

$$H_{i,j-1} \geq H_{i+1,j-1},$$

$$H_{i,j-1} < H_{i,j}. \quad (63)$$

The first three of these equations imply that

$$H_{i,j-1} \geq H_{i+1,j-1} > H_{i+1,j} > H_{i,j}, \quad (64)$$

which is incompatible with the last inequality in Eq. (63). Clearly such a configuration cannot be realized in nature. The root of this problem lies in a conflict of information similar to the phenomenon of frustration encountered in spin systems. Pictorially, these height configurations are reminiscent of the drawing *Ascending and Descending* by M. C. Escher.

In the Appendix we find that only 126 176 configurations generated by Eq. (59) are physical, and, hence, Eq. (59) contains 205 600 "Escher configurations." Naturally the question arises as to whether the appearance of such unphysical height configurations for higher-dimensional substrates is an inherent feature of the WV model or merely an artifact of identity (59). It can be argued [53] that, at least if the WV model is formulated in terms of step functions that compare the heights at two lattice sites, unphysical configurations are unavoidable. However, this does not rule out the possibility of an alternative formulation of the WV model that eliminates contradictions such as in Eq. (63), while preserving Eq. (55) as an identity.

As for the EW model, the rules of the WV model are generalized to continuous height and time variables following the steps in Sec. II A. For the WV model this amounts [53,54,56] to replacing θ_d in Eq. (59) by the representation in Eq. (13) with $a=1$. This is confirmed [51,53,54,56] by comparing the results of KMC simulations of the WV model to solutions of the lattice Langevin equation. Results obtained from the two formulations coincide for $\delta \to \infty$, but excellent agreement is obtained even with a finite δ [53,54]. This again provides the basis for the derivation of an atomistic continuum Langevin equation.

B. Continuum Langevin equation

The presence of unphysical Escher configurations in Eq. (59) leads to some complications when deriving the continuum Langevin equation for the 2D WV model. As a result of the replacement of θ_d by θ in Eq. (13) with a finite δ, Escher configurations give a nonzero contribution and their absence in the transition moments generates nonconserved terms of the form $(\nabla u)^2$ and $(\nabla u)^4$. Such terms correspond to the dissipation of particles and occur because the sum rule in Eq. (55) is no longer satisfied, which fundamentally alters the character of the model. Thus Escher configurations must be included in the expressions for the transition moments, which requires a new rule for particle deposition if such a configuration is encountered. We mandate that in this case the particle stays at the original deposition site. Alternatively, the final deposition site could be selected randomly from all possible target sites, or only from nearest-neighbor sites. The central property of these rules is that they do not violate the symmetry of the model and their effect is to conserve the overall particle number. Any of the aforementioned rules yields the microscopic and coarse-grained behavior of the WV model to be discussed below.

The continuum Langevin equation associated with the WV model is obtained by introducing an analytic height function u according to Eq. (14) and expanding $\theta(\Delta h;\delta)$ in Eq. (15) around $\Delta h=0$ for a finite δ. The substitution of these expressions into the lattice Langevin equation (5) yields a continuum equation which, for small enough δ, contains only terms [51,53,54] that determine fundamental properties of the WV model. Thus we find Eq. (20) as the leading-order continuum Langevin equation for the 1D and 2D WV model. From a practical perspective, the continuum equation for the 2D WV model is derived most conveniently by using the expansions in Eqs. (14) and (15) when calculating the first transition moment in Eq. (48).

Since our atomistic formulation of the WV model is based on a lattice with square symmetry, the continuum Langevin equation for the 2D WV model also embodies this symmetry. As in Sec. III we obtain the simplified form in Eq. (20) by combining terms of the same order of spatial derivatives and powers of u, and averaging over the coefficients of these terms. The leading-order equation (20) is obtained for the WV model if the order of the dominant terms does not decrease as the coarse-graining of height differences through Eq. (13) increases, which restricts δ to $\delta<\delta'$. As for the EW model, the value of δ', as well as the order of the continuum equation, are determined by comparing the maximum magnitudes of the coefficients at different orders in the spatial derivatives. For the 1D WV model such a comparison is carried out in Ref. [54]. Below we focus on the 2D WV model.

Denoting the maximum magnitude of coefficients of terms of order n in the spatial derivatives of $u(x_1,x_2,\tau)$ by $\max[O(n)]$, we find that $\max[O(4)]$ dominates over $\max[O(2)]$ for any δ. Hence the 2D WV model is necessarily described by at least a fourth-order equation at atomistic scales. Due to the computational complexity introduced by the large number of height configurations resolved by the 2D WV model, we only calculate the coefficients of the representative terms $u^{(6,0,0)}(x,y,\tau)$ and $u^{(2,0,0)}(x,y,\tau)u^{(2,2,0)}(x,y,\tau)$ at sixth-order in the spatial derivatives. Comparing the magnitudes of the coefficients of these terms to $\max[O(4)]$, we find that even with $\delta\approx 1$,

$$\max[O(4)] \approx 10 \max[O(6)].$$

Somewhat surprisingly, the magnitude of the coefficient of the nonlinear term $u^{(2,0,0)}(x,y,\tau)u^{(2,2,0)}(x,y,\tau)$ decreases relative to the coefficients of terms of second order and fourth order as δ increases beyond $\delta=1$. However, since the coefficient of $u^{(2,0,0)}(x,y,\tau)u^{(2,2,0)}(x,y,\tau)$ only involves the first two terms in the expansion of θ, both of which stay finite as $\delta\to\infty$, we attribute this to the specific nonlinear term chosen. On this basis we have $\delta'\approx 1$.

The above considerations indicate that the leading-order continuum equation for the WV model is obtained with $\delta<\delta'\approx 1$ for 2D substrates, while we have [54] $\delta<\delta'\approx 0.001$ for 1D substrates. The difference in the upper bound δ' arises because, for 2D substrates, many more step functions need to be multiplied to define a single height configuration, which means that the rapid convergence of the series expansion of θ for small δ has a greater effect on the overall expression for the transition moments. For the EW model, on the other hand, it was found in Sec. III that the value of δ' for $d=2$ is only slightly greater than for $d=1$. This discrepancy between the two models arises because the increase in the number of step functions necessary to define height configurations is (exponentially) greater for the WV model, and because we have taken $a\to 0$ for the EW model, which reduces the effect of higher powers of θ on the coefficients in the continuum equation.

With these bounds on δ, the numerical values of the coefficients in Eq. (20) for the WV model are summarized in Table II. While for 1D substrates the dominance of the term $\nu_4\nabla^4 u$ is independent of the choice for δ (provided that $0<\delta<\delta'$), the situation for 2D substrates is more subtle. Decreasing δ leads to an artificial "crossover" from an equation in which nonlinear terms have coefficients with appreciable magnitudes to an equation dominated by linear terms. This is a result of the representation for θ in Eq. (13) which, for $\delta<1$, reduces the magnitude of nonlinear terms for any growth model. Since the leading-order equation is obtained even with $\delta\approx 1$, and the rules of the WV model are more accurately satisfied for larger values of δ, we set $\delta=1$ in Table II. Indeed, in Ref. [54] close agreement between the lattice Langevin equation for the WV model and KMC simulations is found even with $\delta=1$, albeit for a 1D substrate.

TABLE II. Rounded coefficients in Eq. (20) for the WV model with substrate dimension d. The values are obtained with the representative choices $\delta=10^{-4}$ $(d=1)$ and $\delta=1$ $(d=2)$. We have set $a_\perp=a_\parallel=\tau_0=1$.

d	ν_2	ν_4	λ_{13}	λ_{22}	D_0	D_2
1	2×10^{-9}	5×10^{-5}	-4×10^{-17}	3×10^{-9}	$\frac{1}{2}$	0
2	5×10^{-2}	1×10^{-1}	-4×10^{-2}	-4×10^{-2}	$\frac{1}{2}$	0

The coefficients in Table II indicate that, for 1D substrates, ν_4 is the dominant coefficient. Thus the short-wavelength and high-frequency properties of the 1D WV model are, to a very good approximation, captured by the MH equation (46). This prediction is in excellent agreement with the initial behavior observed in KMC simulations [44,60] and long-standing physical arguments [34,35]. Increasing the dimensionality of the substrate to $d=2$, however, leads to a dramatic change in the relative magnitudes of the coefficients in the continuum Langevin equation. Even at microscopic length and time scales, all the terms in this equation must be considered on an equal footing and the description of fluctuating interfaces produced by the WV model with any one of the standard equations (45)–(47) breaks down. The RG analysis described in the next section will reveal how the distinct behavior of the 1D and 2D WV models, already apparent in the atomistic Langevin equations, persists along the RG trajectories.

C. Renormalization-group trajectories

The entries in Table II demonstrate that all of the terms in Eq. (20) must be retained for the 2D WV model. One might therefore anticipate that the flow trajectory of the two-dimensional WV model is qualitatively different from the one-dimensional case analyzed in Refs. [51,54] as well as from the two-dimensional EW model studied in Sec. III C. This is confirmed by Fig. 4, in which solutions of Eqs. (38)–(42) are plotted as functions of the flow parameter ℓ. In the initial stages of the RG trajectory, the system is described by Eq. (20) with $\nu_2>0$ and $\nu_4>0$. Thus, the surface morphology is smooth during the early stages of growth, which is also expected on the basis of the original physical motivation [10,60,61] of the WV model as a form of nonthermal surface diffusion.

Under repeated RG transformations, however, the negative sign of the coefficient λ_{13} in Eq. (20) changes the sign of the diffusion coefficient ν_2 and our 2D model is eventually described by

$$\frac{\partial u}{\partial \tau} = -|\nu_2|\nabla^2 u - |\nu_4|\nabla^4 u - |\lambda_{13}|\,\boldsymbol{\nabla}(\boldsymbol{\nabla} u)^3 + \lambda_{22}\nabla^2(\boldsymbol{\nabla} u)^2 + \xi, \tag{65}$$

which is manifested in terms of the rescaled variables in Eqs. (33)–(35) by

$$r>1, \quad u_1<0, \quad u_2>0. \tag{66}$$

To understand the physical content of Eq. (65), consider its linearized form, a central feature of which is a critical wave number $k_c=\sqrt{|\nu_2/\nu_4|}$ below which all modes are unstable. The maximally unstable mode $k_m=k_c/\sqrt{2}$ defines a characteristic length $L_m=2\pi/k_m$ that sets the scale for a regular array of islands with diverging heights. This behavior preempts kinetic roughening in this regime. These conclusions are consistent with large-scale computer simulations of the 2D WV model [45], where a mounded surface morphology is observed for long simulation times.

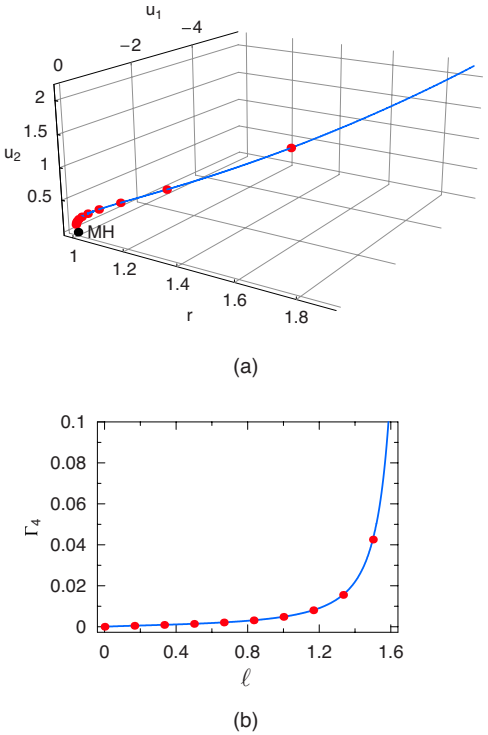

FIG. 4. (Color online) RG flow trajectory of the 2D WV model obtained from Eqs. (38)–(42) with the initial conditions in Table II: (a) RG flow of the deterministic part of Eq. (20) and (b) RG flow of the amplitude of fluctuations with $\Gamma_2=0$ at every point along the RG trajectory. The trajectory starts off not too far from the MH fixed point, but eventually crosses over to a regime for which $r>1$ and $u_2>0$, and becomes unstable. The range of the flow parameter ℓ is the same in panels (a) and (b). Superimposed on the trajectory are points separated by a logarithmic scale of $\Delta\ell=1/6$.

D. Experimental realization

The WV model was originally proposed [61] as a qualitative description of the low-temperature growth of group-IV semiconductors. On this basis we can use the RG trajectory in Fig. 4 to describe recent experiments on the homoepitaxial growth of Ge(001) [30], which observed a low-temperature growth-mode transition from ordered layer-by-layer growth initially to epitaxial breakdown. Atomic force micrographs [30], which are reproduced in Fig. 5, show that the morphology resulting from the deposition of material is smooth initially [Fig. 5(a)], comparable with the smooth buffer layer, followed by the emergence of a regular array of small mounds [Fig. 5(b)], which roughen, coarsen, and become pyramidal [Figs. 5(c) and 5(d)], and the eventual development of hillocks [Fig. 5(e)] that signal epitaxial breakdown and the onset of amorphous growth [Fig. 5(f)].

The self-organization of ultimately unstable islands out of a smooth surface morphology is precisely the pathway predicted by Fig. 4 with Eq. (20) and the coefficients in Table II for the initial transient regime, and Eq. (65) at longer length and time scales. On the level of the continuum Langevin equation (20) this growth-mode transition can be understood in terms of the interplay between ν_2 and λ_{13}, which are argued [41] to have similar effects on the evolution of surface

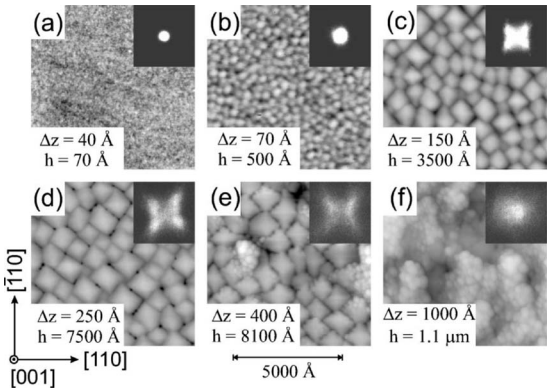

FIG. 5. Atomic force micrographs of the surface of Ge(001) during low-temperature homoepitaxial growth at $T=155$ °C and a growth rate of 0.5 Å s^{-1}. Film thicknesses h and black-to-white grayscales Δz are (a) $h=70$ Å, $\Delta z=40$ Å, (b) $h=500$ Å, $\Delta z=70$ Å, (c) $h=3500$ Å, $\Delta z=150$ Å, (d) $h=7500$ Å, $\Delta z=250$ Å, (e) $h=8100$ Å, $\Delta z=400$ Å, and (f) $h=1.1$ μm, $\Delta z=1000$ Å. The insets show 2D slope histograms, ranging over $\pm 25°$ in the x and y directions, indicating the directions of surface normal vectors. After Ref. [30].

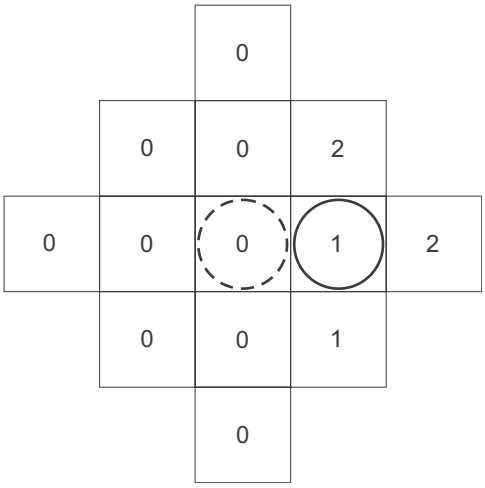

FIG. 6. Plan view of a local height configuration producing an upward jump in the 2D WV model. The initial deposition site is the central site indicated by the dashed circle, the final deposition site is indicated by the solid circle, and the numbers in each square denote the surface height at this lattice site disregarding the newly deposited particle.

profiles. The initial conditions for the 2D WV model imply that $\nu_2>0$ but $\lambda_{13}<0$, with λ_{13} being of appreciable magnitude. The change in the sign of ν_2 with increasing coarse-graining can therefore be interpreted as λ_{13} "winning over" ν_2.

The WV model suggests a simple qualitative explanation for the observed growth-mode transition on Ge(001) [30] in terms of atomistic dynamics. The basic principle defining the WV model is the local maximization of nearest-neighbor bonds. For 1D substrates this implies that a deposited particle always moves to a nearest-neighbor site that has the same or lower height than the original deposition site, regardless of the roughness of the surface (see Figs. 4 and 5 of Ref. [56]). The same is true for the EW model (see Fig. 1 of Ref. [56]), so one might expect that the two models belong to the same universality class. This is confirmed by the RG trajectories in Fig. 1 of the present paper and Fig. 5 of Ref. [54], although the transient behavior of the two models is rather different.

For 2D substrates, however, the rules of the WV model allow particles to jump *up* for particular local configurations near steps. This is illustrated in Fig. 6 for a representative height configuration. In the early stages of growth, when the surface is fairly smooth in that there are large terraces on which there are few atoms, arriving atoms are incorporated at the same or lower layer as the original deposition site. Such transitions promote smooth growth, as is observed experimentally [30,90]. The continuum growth equation (20) with the coefficients in Table II supports this. But, as the surface roughens due to the shot noise produced by the deposition flux, configurations composed of steps upon steps become more likely, which leads to the appearance of local configurations that, according to the transition rules of the 2D WV model, favor deposition to a *higher* layer than the deposition site (see Fig. 6). As noted earlier, the height of the target layer is thereby immaterial for the transition rate. This might amplify the instability in the later stages of growth, where there is an increasing likelihood of substantial height differences between neighboring sites. However, the main point is that, as observed previously in KMC simulations of the 2D WV model [45], the fact that upward jumps are allowed for the 2D WV model leads to the development of competing downward *and* upward currents and, hence, to the emergence of a characteristic length scale and self-organized mounds. This behavior is reflected in the RG flow of the 2D WV model shown in Fig. 4, which provides a stark contrast to the RG trajectory of the 2D EW model in Fig. 2.

V. ACTIVATED SURFACE DIFFUSION

Highly simplified atomistic descriptions of growth, such as the EW and WV models studied in Secs. III and IV, are often employed as prototype models in the statistical mechanics community. Such models can, at best, capture the qualitative evolution of surface morphologies observed in experiments. More realistic descriptions of homoepitaxial growth must involve material-specific parameters to account for local bonding configurations and growth parameters such as the substrate temperature and deposition flux. One of the simplest stochastic lattice models of homoepitaxial growth which is capable of a *quantitative* description of experiments [21–23] is the diffusion model described in Sec. II. A basic expression for $E_{i,j}$ is obtained as the sum of a site-independent energy barrier E_S from the substrate and a contribution E_N from each of the $n_{i,j}$ lateral nearest neighbors: $E_{i,j}=E_S+n_{i,j}E_N$. More distant neighbors may be included for the calculation of $E_{i,j}$, in which case atomic interactions based on model potentials are sometimes used to avoid a proliferation of parameters. For comparisons with the morphologies of specific materials systems, these barriers can be determined either by fits to a particular experiment [21–23] or from first-principles calculations [24].

The simplest way of modeling the deposition flux is to include the random deposition of particles at a rate $1/\tau_0$. The renormalization of the resulting lattice model is described in detail in Refs. [52,53]. Taking the continuum limit of the lattice Langevin equation according to Sec. II, one obtains [52,53] the Langevin equation (20) as the basic continuum description of the above model. For 1D and 2D substrates the coefficients in Eq. (20) appropriate for our model are [52]

$$\nu_2 = \lambda_{13} = 0 \tag{67}$$

due to the symmetry of the underlying atomistic processes, and

$$\nu_4 = -\frac{a_\parallel^4}{a_\perp^2}\frac{D_S}{2d}B\gamma(1-A\gamma)^{2d-1}, \tag{68}$$

$$\lambda_{22} = -\frac{a_\parallel^4}{a_\perp^3}\frac{D_S}{2d}\gamma(1-A\gamma)^{2d-2}[B^2\gamma + 2C(1-A\gamma)], \tag{69}$$

$$D_0 = a_\parallel^d \frac{a_\perp^2}{2\tau_0}, \tag{70}$$

$$D_2 = a_\parallel^{d+2}\frac{D_S}{2d}(1-A\gamma)^{2d}, \tag{71}$$

where the leading-order equation is obtained with $\delta < \delta' \approx 0.02$, such that $A \approx 0.5$, $B \approx 0.006$, and $C \approx -3\times 10^{-7}$ in Eq. (15) for $\delta \approx 0.01$, and

$$\gamma = 1 - e^{-\beta E_N},$$

$$D_S = a_\perp^2 \nu_0 e^{-\beta E_S}. \tag{72}$$

Coefficients of higher-order terms have smaller magnitudes than those retained in Eqs. (20) and (21) and, thus, can be regarded as being negligible for the purpose of a perturbative RG analysis. In contrast to the EW and WV models, the leading-order equation for surface diffusion has full rotational symmetry even though the underlying model is defined on a cubic lattice. This can be understood by noting that, in our description of surface diffusion, the transition rates depend only on the initial site, rather than on the initial *and* the target site.

Using Eqs. (67)–(71) as initial conditions for the RG equations (38)–(42) or the RG equations in Ref. [42], one obtains a sequence of coarse-grained representations of our model for random deposition and surface diffusion. Figure 7 illustrates two such RG trajectories, calculated with the parameter values used in Ref. [63] and two different temperatures. Superimposed on the trajectories are points separated by a logarithmic scale of $\Delta\ell = 1/4$.

The trajectory obtained for $T=500$ K [Fig. 7(a)] starts off close to the MH fixed point before crossing over to the VLDS fixed point. The trajectory at $T=750$ K [Fig. 7(b)], on the other hand, shows a crossover from the cMH to the MH equation, followed by a final crossover to the VLDS equation. For both temperatures the trajectories linger near the MH and VLDS fixed points, but, for the trajectory at $T=750$ K, the flow away from the cMH fixed point is quite

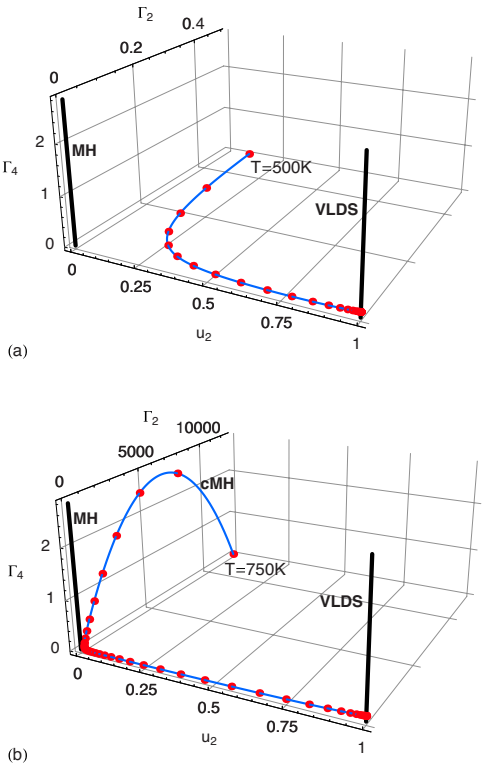

FIG. 7. (Color online) RG trajectories for random deposition with surface diffusion obtained from Eqs. (38)–(42) with the initial conditions in Eqs. (67)–(71) for $d=2$ with [63] $\nu_0 = 5\times 10^{12}$ s^{-1}, $E_S = 1.3$ eV, $E_N = 0.24$ eV, $\tau_0 = 1$ s, and (a) $T=500$ K and (b) $T=750$ K. We have $r=1$ and $u_1 = 0$ everywhere along the RG trajectories. The RG flow is always directed toward the VLDS fixed point and the points superimposed on the trajectories are separated by a logarithmic scale of $\Delta\ell = 1/4$.

rapid. Indeed, close to a given fixed point, values of $\Delta\ell$ can be related [53,54] to time intervals $\Delta\tau$ via $\Delta\tau = e^{z\Delta\ell}$. The cMH and MH fixed points have a dynamic exponent $z=4$, and the VLDS fixed point has $z=10/3$ for $d=2$ [10,41]. Thus the trajectories in Fig. 7 imply a rapid flow away from the cMH fixed point, but an extended residence time near the MH fixed point with a relatively slow approach of the VLDS fixed point. A more quantitative estimate of crossover times implied by RG trajectories could be obtained from a more sophisticated measure of the degree of coarse-graining, for example, by using the correlation length associated with each point along a RG trajectory [53,54,99].

The crossovers in Fig. 7 illustrate the inherent difficulties encountered [31–33,48,49] when attempting to describe growth morphologies observed in experiments on the basis of postulated continuum equations. Even if there is reason to expect that the morphological evolution of a system is described by the VLDS equation, our and previous [41,42] RG analyses show that this is only an *asymptotic* fixed point. Transient regimes, where experiments are most often carried out, are described by the MH equation in the case of random deposition with concurrent surface diffusion.

Depending on the choice for the material-specific parameters ν_0, E_S, and E_N, and the growth parameters T and τ_0, different starting points of the RG flow and, hence, different

RG flow trajectories are obtained [52,53]. Excellent agreement between RG trajectories [52,53] and KMC simulations of this model [44,63] is found for all available parameter values and simulation times. An extended residence time near a given fixed point is manifested as a scaling behavior characteristic of that fixed point in computer simulations [44,63]. A crucial difference between the EW and WV models and random deposition with surface diffusion lies in the asymptotic behavior: Random deposition with surface diffusion is described asymptotically by the VLDS equation (47) for 1D *and* 2D substrates [52]. This raises a number of interesting issues when surface diffusion is combined with the WV model, as will be discussed in the next section.

VI. WOLF-VILLAIN MODEL WITH ACTIVATED SURFACE DIFFUSION

The results in Sec. IV confirm that the WV model provides a basic qualitative description of the short-range nonthermal motion of newly deposited particle species. For the 2D WV model we obtain a dramatic transition from smooth to unstable growth, which is also observed in experiments [30]. But in any growth experiment, the finite temperature of the substrate induces a nonzero transition rate for thermally activated surface diffusion. What effect does a finite surface temperature have on the growth-mode transition of the 2D WV model? In this section, we study a model that combines the WV model with the diffusion model of Sec. V [100] to investigate the effect of finite substrate temperatures on the growth-mode transition predicted by the WV model. We comment in passing here that performing the corresponding KMC simulations would require substantial computational resources, in addition to those already required for large-scale simulations of the 2D WV model alone [44,45].

A. Continuum Langevin equation

The lattice Langevin equation for the WV model with surface diffusion is obtained in direct analogy with the derivation of the lattice Langevin equation for the WV model in Sec. IV and the analytic formulation of surface diffusion and random deposition in Sec. V. The WV deposition rules thereby replace the random deposition of particles in Sec. V. Hence, the first and second moments of the combined model are obtained by adding the transition moments for surface diffusion in Eqs. (9) and (10), and the transition moments in Eqs. (48) and (49) for the WV model. This completely specifies the lattice Langevin equation (5) for the WV model with surface diffusion in $d=1$ and 2.

The continuum Langevin equation for the WV model with surface diffusion is obtained by taking the continuum limit of the lattice Langevin equation (5) according to Sec. II B. We thus find that the leading-order Langevin equation for the WV model with surface diffusion is given by Eq. (20). As for the 2D WV model, this equation exhibits only square symmetry rather than full rotational symmetry. We obtain the simplified form in Eq. (20) by combining terms arising from the WV rules as described in Sec. IV B. As noted above, the 2D diffusion model exhibits full rotational symmetry, so terms arising from the diffusion rules are automatically of the form in Eq. (20). Expressions for the coefficients are obtained by adding the contributions from the WV model and surface diffusion. Thus, we find that Eq. (20) provides a description for thermally activated surface diffusion, mobility induced by the heat of condensation, and the random deposition of particles.

The leading-order Langevin equation (20) is obtained if the order of the dominant terms does not decrease as the coarse-graining of height differences through Eq. (13) increases, which restricts δ to $\delta<\delta'$. As for surface diffusion with random deposition and the WV model, the value of δ', as well as the order of the continuum equation, are determined by comparing the maximum magnitudes of the coefficients at different orders in the spatial derivatives. Since the effect of δ is to smoothen height differences [53,54], the *same* value of δ must be used for all processes appearing in the combined model. This means that, although we have already obtained leading-order equations for the WV model (Sec. IV) and surface diffusion (Sec. V), the range of δ must be determined anew for the combined lattice model.

1. One-dimensional substrates

For illustration, consider the values of the diffusion parameters in Ref. [63]. We find that the leading-order continuum Langevin equation for the WV model with surface diffusion is dominated by contributions originating from the 1D WV model in Eq. (20) with the coefficients in Table II for $T\lessapprox 500$ K, and by the contributions in Eqs. (67)–(71) with $\tau_0\to\infty$ for the diffusion model in the regime $T\gtrapprox 650$ K. Between these temperature ranges is a regime for which the leading-order Langevin equation involves the same terms of second- and fourth-order spatial derivatives as for the WV and diffusion models, but with coefficients which receive significant contributions from both models. Considering that for surface diffusion $\delta<\delta'\approx 0.02$, we use the same range of δ for the combined model as for the 1D WV model alone, i.e., $\delta<\delta'\approx 0.001$.

2. Two-dimensional substrates

Again consider the values for the diffusion parameters in Ref. [63]. Similar to the 1D model, the leading-order continuum equation for the 2D WV model with surface diffusion is dominated by terms corresponding to the 2D WV model for $T\lessapprox 500$ K, and by terms corresponding to the diffusion model for $T\gtrapprox 650$ K, with a smooth intermediate regime between these temperature ranges. In particular, for the diffusion dominated regime we have

$$\max[O(2,4)]\gtrapprox 1\ \max[O(6)] \quad \text{for} \quad \delta\lessapprox 0.9,$$

$$\max[O(2,4)]\gtrapprox 10\ \max[O(6)] \quad \text{for} \quad \delta\lessapprox 0.1$$

for the deterministic terms, and

$$\max[D_0,D_2]\gtrapprox 1\ \max[O(2)] \quad \text{for} \quad \delta\lessapprox 1,$$

$$\max[D_0,D_2]\gtrapprox 10\ \max[O(2)] \quad \text{for} \quad \delta\lessapprox 0.02$$

for the amplitude of fluctuations obtained from $K^{(2)}$. Even for $\delta\approx 1$, however, the continuum equation for the diffusion

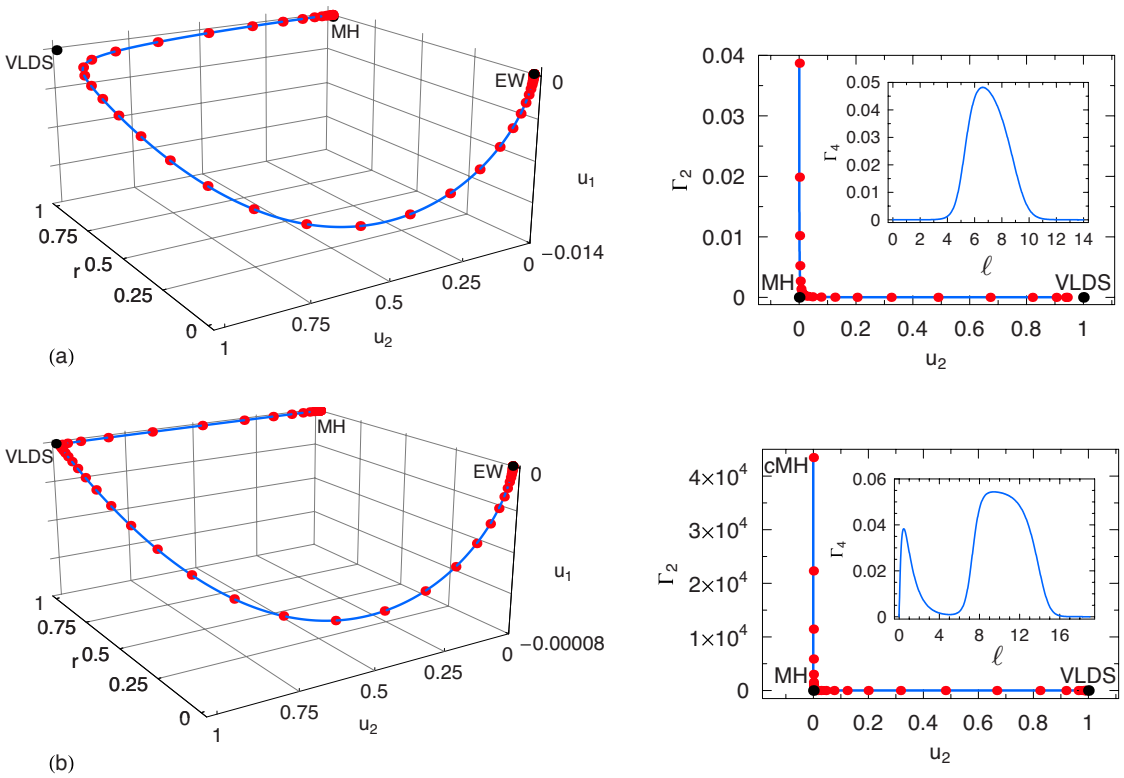

FIG. 8. (Color online) RG flow trajectories of the 1D WV model with surface diffusion for (a) $T=300$ K and (b) $T=500$ K obtained from Eqs. (38)–(42) with the initial conditions in Table II and Eqs. (67)–(71) with $\tau_0 \to \infty$ and $\delta=10^{-4}$. For thermally activated diffusion we use $\nu_0=5\times10^{12}$ s^{-1}, $E_S=0.9$ eV, and $E_N=0.2$ eV. In both (a) and (b) the RG flow is directed away from the MH or cMH fixed point, and superimposed on the RG trajectories are points separated by $\Delta\ell=1/3$. The range of the flow variable ℓ is identical in the left and right panels, with the exception of the plots of Γ_2 vs u_2, in which the RG trajectories are only plotted up to the turning point away from the VLDS fixed point.

model implies a similar behavior under RG transformations as for $\delta<0.02$, which is the range used in Sec. V and Ref. [54]. This robustness of the diffusion model allows us to use $\delta\approx1$ for the WV model with surface diffusion at all temperatures.

3. Numerical values of coefficients

On the basis of the foregoing considerations we obtain the leading-order continuum Langevin equation (20) for the WV model with surface diffusion with $\delta<\delta'\approx0.001$ for 1D substrates, and with $\delta<\delta'\approx1$ for 2D substrates. The difference in the upper bounds on δ for $d=1$ and 2 is for similar reasons as discussed in Sec. IV. Moreover, as in Sec. IV, we also use $\delta\approx1$ for the 2D WV model with surface diffusion such that nonlinear terms are not artificially suppressed. Thus the coefficients of the WV model with surface diffusion are given by the sum of the values in Table II for the WV model and Eqs. (67)–(71) of Sec. V with $\tau_0\to\infty$ for surface diffusion, with the representative choices $\delta=10^{-4}$ for $d=1$ and $\delta=1$ for $d=2$.

B. Renormalization-group trajectories

Figure 8 shows RG trajectories for the 1D WV model with surface diffusion at two temperatures. For $T\approx300$ K [Fig. 8(a)] the trajectory is essentially identical to that of the 1D WV model in Fig. 5 of Ref. [54]. Surface diffusion does not affect the crossover of the 1D WV model, but for high enough substrate temperatures, shifts the initial conditions toward the MH equation with conserved noise. This is illustrated in Fig. 8(b) for $T=500$ K. As a result, the RG flow is "delayed" through extended residence times near the cMH fixed point and the MH fixed point. Moreover, as can be seen from Fig. 8(b), the presence of strong surface diffusion also leads to a more pronounced approach of the VLDS fixed point. This is consistent with the VLDS fixed point providing the asymptotic description for random deposition with surface diffusion (Sec. V).

Figure 9 shows RG trajectories for the 2D WV model with surface diffusion. Similar to the 2D WV model, these trajectories always flow into a regime described by Eq. (65). For $T=400$ K [Fig. 9(a)] we obtain essentially the same RG trajectory as for the 2D WV model in Fig. 4, whereas for $T=500$ K [Fig. 9(b)] surface diffusion modifies the RG trajectory of the WV model. The WV model with surface diffusion is therefore more sensitive to changes in temperature for $d=2$ than for $d=1$. The RG trajectory in Fig. 9(b) exhibits several intriguing features. First, this trajectory indicates that at higher temperatures surface diffusion delays the instability of the 2D WV model through extended residence times near the cMH fixed point and the MH fixed point corresponding to Eq. (46). Indeed, we have $z=4$ for both the MH and the cMH equations [10], which suggests that for high

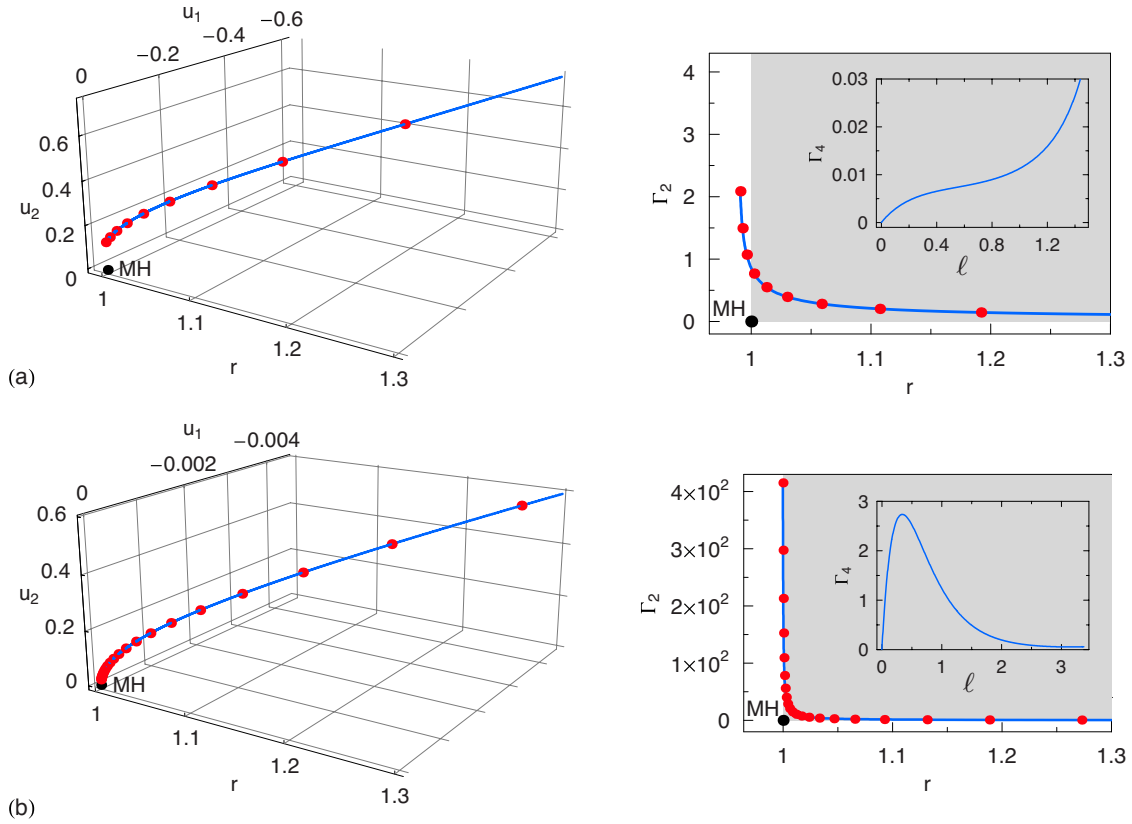

FIG. 9. (Color online) RG flow trajectories of the 2D WV model with surface diffusion for (a) $T=400$ K and (b) $T=500$ K obtained from Eqs. (38)–(42) with the initial conditions in Table II and Eqs. (67)–(71) with $\tau_0 \to \infty$ and $\delta=1$. For thermally activated diffusion we use $\nu_0=5\times10^{12}$ s^{-1}, $E_S=0.9$ eV, and $E_N=0.2$ eV. In both (a) and (b) the RG flow is directed toward increasing values of r, and superimposed on the RG trajectories are points separated by $\Delta\ell=1/6$. The range of the flow variable ℓ is identical in the left and right panels. The shaded region corresponds to $r>1$ and $u_2>0$, for which Eqs. (33) and (35) imply $\nu_2<0$ and $\nu_4>0$.

enough temperatures the 2D WV model with surface diffusion would show a pronounced kinetic roughening regime.

We also note that for large values of T the atomistic Langevin equation is dominated by the terms describing surface diffusion. As shown in Sec. V the asymptotically stable fixed point for surface diffusion with random deposition is the VLDS fixed point for $d=1$ *and* 2. Therefore one might expect that the VLDS fixed point is at least approached as a transient fixed point in the diffusion dominated regime for $d=2$, as it is for $d=1$. As shown in Fig. 9(b), however, the terms $\nu_2\nabla^2 u$ and $\lambda_{13}\boldsymbol{\nabla}(\boldsymbol{\nabla}u)^3$, although seemingly negligible at microscopic scales for high enough temperatures, carry the system directly from the MH regime into an unstable regime. This further highlights the previous observation [45,46,58] that even supposedly innocuous modifications of atomistic transition rates can have highly nontrivial consequences. Considering that there is usually some arbitrariness involved in the formulation of lattice models, this makes an analytic approach of the type described in this paper essential.

VII. DISCUSSION

The system of RG equations (38)–(42), together with the initial conditions in Tables I and II and Eqs. (67)–(71), provide continuum descriptions of the EW and WV models and surface diffusion for any length and time scales—from the atomistic resolution of the original transition rules to the macroscopic realm. The parameters in these coarse-grained continuum equations are determined by the underlying lattice model and, hence, a direct comparison between continuum equations and growth experiments becomes feasible. In particular, our procedure can be used to predict *transient* surface morphologies as a function of the growth conditions, which is important for modeling device fabrication [31,32]. The lattice Langevin equation (5) thereby relates the coefficients in the continuum descriptions to the atomistic transition rules of the lattice models at any point along the RG trajectories. Equations (5), (20), and (38)–(42) therefore establish a first-principles multiscale description of the EW and WV models and our model for surface diffusion. The results obtained using this methodology are found to be in agreement with all available computer simulations of these models and provide an explanation of recent low-temperature experiments [30] of homoepitaxy on Ge(001).

An important practical point is that, since KMC simulations of even relatively simple lattice models, such as the EW and WV models, can require substantial computational resources [45,46], even for one-dimensional substrates [44,62], our method can help to clarify incomplete or ambiguous results. Thus, our multiscale method can be viewed as an augmentation of KMC simulations which could, for

instance, be used to lend analytic support to acceleration methods employed in computer simulations. Moreover, once a set of atomistic processes has been renormalized, it is straightforward to obtain a multiscale theory of models combining the different atomistic processes. This is in stark contrast to computational approaches for which all simulations would have to be repeated for the combined model. In fact, following the approach presented here, it becomes possible to establish a direct quantitative link between regions in growth parameter space and transient and/or asymptotic regimes of morphological evolution. This raises the possibility of identifying a range of growth conditions and material parameters that produce a specified surface morphology at particular length and time scales.

We demonstrated in Secs. IV and VI that for 2D substrates the WV deposition rules imply that the coefficient ν_2 in Eq. (20) changes sign under coarse-graining. Indeed, Figs. 4 and 9 show that the flow away from the MH fixed point becomes very rapid, indicating unstable behavior. Eventually, the RG equations become too stiff to allow numerical solutions with standard algorithms implemented in software packages such as MATHEMATICA or MATLAB. It is not clear at this stage whether the RG trajectories of the 2D WV model and the 2D WV model with surface diffusion indeed diverge as $\ell \to \infty$. Thus, the detailed mathematical investigation of the RG equations (38)–(42) with the initial conditions in Table II for $d=2$ remains an open problem. Considering that the negative sign of ν_2 leads to unstable behavior, however, epitaxial growth is expected to break down in the regime with $r>1$ and $u_2>0$, which is also observed in the experiments in Ref. [30]. After the breakdown of epitaxial growth the structure of the growing film is found to be amorphous [30], which suggests that in this regime it is necessary to describe the atomistic dynamics on the basis of nonconserved growth models [10,53,85]. This makes it unlikely that the asymptotic behavior of the 2D WV model is of relevance for such experiments.

There are several immediate extensions to the work reported here. Computer simulations have indicated [44–46] that ostensibly trivial modifications of the transition rules of the EW and WV models can lead to profound changes in the scaling behavior. Using the first-principles multiscale approach described in this paper the effects of such modifications can be systematically studied and the origin of any changes in the morphology produced by the model identified. In particular, as described in Sec. III a possible origin of the anomalies observed for the EW model is the positive overall positive sign of the term $\nu_4\nabla^4 u$ in Eq. (20), which is stabilized by the term $\nu_6\nabla^6 u$ through Eq. (56). Such studies of model systems are useful for providing challenges that enable us to test and extend our methodology.

On the other hand, any quantitative comparison to epitaxial growth experiments necessitates including transition processes associated with particular features of systems, such as surface diffusion, desorption, step-edge diffusion, and step-edge barriers to interlayer adatom migration. For example, there is substantial experimental data for island-size distributions in the submonolayer regime and on the role of multiple species in the epitaxial growth of compounds. KMC simulations for these scenarios are quite well-developed and capable of detailed comparisons with experiment [23,24,101–103]. Lattice Langevin equations can produce results that are statistically equivalent to KMC simulations, so expansions of these equations could provide a systematic analytic framework to augment this simulation work. Moreover, since the rates of many surface processes can now be calculated with density functional [24] and molecular dynamics [25] methods, the opportunity is presented of a truly first-principles "atoms-to-continuum" multiscale methodology, in which the macroscopic expression of atomistic processes can be determined and compared with real materials systems. Such an approach would raise our method to a new level by connecting macroscopic physics directly to the smallest length and time scales accessible with current technology.

Another application for which our multiscale approach could have useful practical and conceptual consequences is heteroepitaxial growth. Due in large measure to the promise of many technological innovations, much effort has been devoted to the description of self-organized quantum dot formation during the heteroepitaxial growth of lattice mismatched systems. This presents an especially acute challenge for most theoretical methods because of the relaxation of misfit strain, which introduces long-range elastic interactions and preempts purely local estimates of kinetic barriers. Nevertheless, KMC simulations that incorporate elastic effects to various levels of sophistication [104–106] suggest that including a contribution from the local elastic energy to the kinetic barriers for detachment and migration provides a useful starting point for understanding strain-induced morphologies.

Indeed, in Ref. [88] we used the approach described in this paper to derive the leading-order continuum equation for a "minimal" atomistic model of heteroepitaxial growth. Interestingly, the deterministic part of this Langevin equation has the same form as obtained previously [107] completely within the framework of continuum elasticity. On this basis, one can begin to contemplate a direct relation between atomistic and continuum modeling methodologies for the self-organization of nanostructures, and relate continuum elasticity to atomistic interactions. Such an approach would combine the computational advantages of continuum equations with the atomic resolution of lattice models, and could facilitate the ultimate aim [8] of specifying the growth conditions under which stable and regular arrays of structures with well-defined shapes are produced at the nanoscale.

VIII. SUMMARY AND CONCLUSIONS

Using the general multiscale method for stochastic lattice models described in a companion paper [54], we have obtained hierarchies of Langevin equations describing prototypical models of homoepitaxial surface growth over expanding length and time scales. Our analysis points to the following intriguing conclusion: The morphological manifestation of an atomistic relaxation mechanism, such as the local maximization of nearest-neighbor bonds, can depend crucially on the dimensionality of the system and on the length and time scales considered. For the WV model this is evi-

denced by the qualitatively different surface morphologies for 1D and 2D substrates and, for 2D substrates, by the transition from smooth surface morphologies to self-organized arrays of islands. These results are consistent with KMC simulations [44–46,63] of the models studied in this paper.

The sequence of fixed points approached by a given lattice model depends not only on the general structure and symmetry of the microscopic equation, but also on the numerical values of the coefficients corresponding to the initial point of the RG trajectory. For the models considered here, this is apparent from the very different transient morphologies produced by the EW model, the WV model, surface diffusion with random deposition, and the WV model with surface diffusion. These models are all described initially by Eq. (20), so the pronounced differences in their transient and macroscopic properties are due solely to the initial values of the coefficients. The direct derivation of the underlying microscopic Langevin equation coupled with a dynamic RG analysis is capable of capturing this behavior. The multiscale approach employed in this paper opens the door to similar investigations of all types of stochastic lattice models which can be described in terms of master equations.

ACKNOWLEDGMENTS

This work was supported at Imperial College London by funds from the U.K. Engineering and Physical Sciences Research Council and the European Commission Sixth Framework Programme as part of the European Science Foundation EUROCORES Programme on Self-Organized Nanostructures (SONS). C.A.H. was supported at MIT by the Austrian Science Fund and thanks M. Kardar and R. J. Phaneuf for interesting discussions.

APPENDIX: ALGORITHMIC COMPUTATION OF TRANSITION MOMENTS

In this appendix we describe the automated calculation of transition moments using symbolic computation software. All calculations are illustrated for the 2D WV model, but the method is readily generalized. Our main consideration when formulating the algorithm is to mirror the physical processes involved as closely as possible in the calculation. This concern takes precedence over efficiency of computation. Each configuration generated by Eq. (59) is considered separately and allocated to one of the local transition rates according to the rules of the discrete model.

We first introduce a coordinate system for labeling the height of the substrate at the initial deposition site and its neighbors. These coordinates will be used as dummy variables and the labeling convention is summarized in Fig. 10. The step function appearing in Eq. (59) can then be redefined as

$$\theta_d(H_{i+1,j}-H_{i+2,j}) \to \theta_d(H_{i+1,j}-H_{i+2,j})\mathrm{UnitStep}[D_N-D_{NN}], \tag{A1}$$

with analogous definitions for all other height variables. In these expressions UnitStep$[x]$ is a representation of the step function $\theta_d(x)$ in Eq. (12) in MATHEMATICA [97]. The left-hand side of Eq. (59) contains all configurations we need to consider and will therefore be denoted by $\mathcal{C}_T(\{D\})$ where $\{D\}$ is shorthand for the set of variables $(D,D_N,\ldots,D_{EE})$.

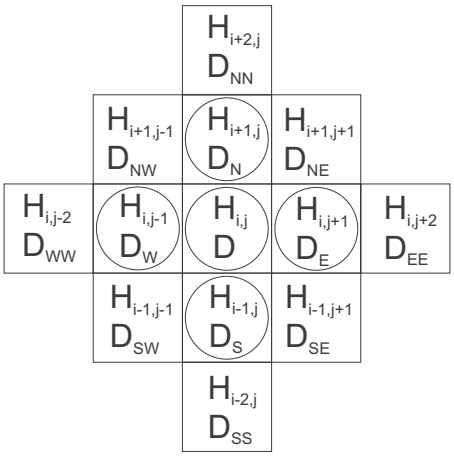

FIG. 10. Plan view of the relevant height variables for the 2D WV model. The initial deposition site has height $(H_{i,j},D)$, and any of the sites marked with a circle may be selected as the final deposition site.

Our basic method is to allocate the various configurations that constitute the total height configurations $\mathcal{C}_T$ to the different local transition rates by evaluating

$$\sum_{\{D\}} R(\cdot;\{D\})\ \mathcal{C}_T(\{D\}), \tag{A2}$$

where the selection rule $R(H_{i,j};\{D\})$ is equal to one if $\{D\}$ is such that, according to the rules of the WV model, the particle stays at the initial deposition site and equal to zero otherwise. The rules $R(H_{i\pm1,j};\{D\})$ and $R(H_{i,j\pm1};\{D\})$ are defined in direct analogy. The sum $\Sigma_{\{D\}}$ in Eq. (A2) is to be taken over all height configurations $\{D\}$ which are resolved by Eq. (59). In the case of the WV model $\Sigma_{\{D\}}$ can be schematically written as

$$\begin{aligned}\sum_{\{D\}} = &\sum_{D_N,D_E,D_S,D_W=D-4}^{D+4} \sum_{D_{NE}=\min(D_N,D_E)}^{\max(D_N,D_E)+1} \sum_{D_{SE}=\min(D_S,D_E)}^{\max(D_S,D_E)+1} \\ &\times \sum_{D_{SW}=\min(D_S,D_W)}^{\max(D_S,D_W)+1} \sum_{D_{NW}=\min(D_N,D_W)}^{\max(D_N,D_W)+1} \sum_{D_{NN}=D_N}^{D_N+1} \sum_{D_{WW}=D_W}^{D_W+1} \\ &\times \sum_{D_{SS}=D_S}^{D_S+1} \sum_{D_{EE}=D_E}^{D_E+1} d(\{D\}),\end{aligned} \tag{A3}$$

where we have set $a_\perp=1$ and $d(\{D\})$ is a degeneracy factor which ensures that each physical height configuration appearing in $\mathcal{C}_T$ is considered once and only once when evaluating Eq. (A3).

The degeneracy factor is obtained by carefully examining the height configurations generated by the summations in

Eq. (A3) and the symmetries involved. Given $d(\{D\})$ one can obtain an expression for all physical height configurations $\mathcal{C}_P$ by evaluating

$$\mathcal{C}_P = \sum_{\{D\}} \mathcal{C}_T(\{D\}), \tag{A4}$$

from which one finds that $\mathcal{C}_P$ contains 126 176 distinct local height configurations. A useful check of the expression for $d(\{D\})$ is obtained by calculating

$$\sum_{H_{i\pm1,j}=H_{i,j}-4}^{H_{i,j}+4} \sum_{H_{i,j\pm1}=H_{i,j}-4}^{H_{i,j}+4} \sum_{H_{i\pm1,j\pm1}=H_{i,j}-4}^{H_{i,j}+5} \sum_{H_{i\pm2,j}=H_{i\pm1,j}}^{H_{i\pm1}+1} \times \sum_{H_{i,j\pm2}=H_{i,j\pm1}}^{H_{i,j\pm1}+1} |1-\mathcal{C}_P|. \tag{A5}$$

Provided that a suitable expression for $d(\{D\})$ is used in the calculation of $\mathcal{C}_P$ in Eq. (A4) one finds that the above expression is equal to zero, and, hence, that $\mathcal{C}_P$ contains each physical configuration included in $\mathcal{C}_T$ exactly once.

[1] B. A. Joyce, Rep. Prog. Phys. **48**, 1637 (1985).
[2] J. Y. Tsao, *Materials Fundamentals of Molecular Beam Epitaxy* (Academic, Boston, 1993).
[3] M. A. Herman and H. Sitter, *Molecular Beam Epitaxy: Fundamentals and Current Status*, 2nd ed. (Springer-Verlag, Berlin, 1996).
[4] A. Pimpinelli and J. Villain, *Physics of Crystal Growth* (Cambridge University Press, Cambridge, England, 1999).
[5] I. V. Markov, *Crystal Growth for Beginners: Fundamentals of Nucleation, Crystal Growth and Epitaxy*, 2nd ed. (World Scientific, Singapore, 2003).
[6] T. Michely and J. Krug, *Islands, Mounds and Atoms: Patterns and Processes in Crystal Growth Far From Equilibrium* (Springer-Verlag, New York, 2004).
[7] *Atomistic Aspects of Epitaxial Growth*, edited by M. Kotrla, N. Papanikolaou, D. D. Vvedensky, and L. T. Wille (Kluwer, Dordrecht, 2002).
[8] D. D. Vvedensky, in *Low-Dimensional Semiconductor Structures: Fundamentals and Device Applications*, edited by K. Barnham and D. D. Vvedensky (Cambridge University Press, Cambridge, England, 2001), pp. 1–55.
[9] A. Madhukar, Surf. Sci. **132**, 344 (1983).
[10] A.-L. Barabási and H. E. Stanley, *Fractal Concepts in Surface Growth* (Cambridge University Press, Cambridge, England, 1995).
[11] T. Halpin-Healy and Y.-C. Zhang, Phys. Rep. **254**, 215 (1995).
[12] J. Krug, Adv. Phys. **46**, 139 (1997).
[13] *Theory and Applications of Cellular Automata*, edited by S. Wolfram (World Scientific, Singapore, 1986).
[14] T. Toffoli and N. Margolus, *Cellular Automata Machines* (MIT Press, Cambridge, MA, 1987).
[15] Lattice Gas, in *Theory, Application, and Hardware*, edited by G. D. Doolen (MIT Press, Cambridge, MA, 1991).
[16] D. H. Rothman and S. Zaleski, *Lattice-Gas Cellular Automata: Simple Models of Complex Hydrodynamics* (Cambridge University Press, Cambridge, England, 1997).
[17] B. Chopard and M. Droz, *Cellular Automata Modeling of Physical Systems* (Cambridge University Press, Cambridge, England, 1998).
[18] N. Gershenfeld, *The Nature of Mathematical Modelling* (Cambridge University Press, New York, 1999), Chap. 9.
[19] D. D. Vvedensky, Surf. Interface Anal. **31**, 627 (2001).
[20] D. D. Vvedensky, J. Phys.: Condens. Matter **16**, R1537 (2004).
[21] T. Shitara, D. D. Vvedensky, M. R. Wilby, J. Zhang, J. H. Neave, and B. A. Joyce, Phys. Rev. B **46**, 6815 (1992).
[22] T. Shitara, D. D. Vvedensky, M. R. Wilby, J. Zhang, J. H. Neave, and B. A. Joyce, Phys. Rev. B **46**, 6825 (1992).
[23] M. Itoh, G. R. Bell, A. R. Avery, T. S. Jones, B. A. Joyce, and D. D. Vvedensky, Phys. Rev. Lett. **81**, 633 (1998).
[24] P. Kratzer and M. Scheffler, Phys. Rev. Lett. **88**, 036102 (2002).
[25] M. Basham, P. A. Mulheran, and F. Montalenti, Surf. Sci. **565**, 289 (2004).
[26] S. Clarke and D. D. Vvedensky, Phys. Rev. Lett. **58**, 2235 (1987).
[27] A. Madhukar and S. V. Ghaisas, Crit. Rev. Solid State Mater. Sci. **14**, 1 (1988).
[28] H. Metiu, Y.-T. Liu, and Z. Zhang, Science **255**, 1088 (1992).
[29] J. E. Van Nostrand, S. J. Chey, M.-A. Hasan, D. G. Cahill, and J. E. Greene, Phys. Rev. Lett. **74**, 1127 (1995).
[30] K. A. Bratland, Y. L. Foo, J. A. N. T. Soares, T. Spila, P. Desjardins, and J. E. Greene, Phys. Rev. B **67**, 125322 (2003).
[31] H.-C. Kan, S. Shah, T. T. Tadyyon-Eslami, and R. J. Phaneuf, Phys. Rev. Lett. **92**, 146101 (2004).
[32] H.-C. Kan, R. Ankam, S. Shah, K. M. Micholsky, T. Tadayyon-Eslami, L. Calhoun, and R. J. Phaneuf, Phys. Rev. B **73**, 195410 (2006).
[33] T. Tadayyon-Eslami, H.-C. Kan, L. C. Calhoun, and R. J. Phaneuf, Phys. Rev. Lett. **97**, 126101 (2006).
[34] C. Herring, in *The Physics of Powder Metallurgy*, edited by W. E. Kingston (McGraw-Hill, New York, 1951), pp. 143–179.
[35] W. W. Mullins, J. Appl. Phys. **28**, 333 (1957).
[36] S. F. Edwards and D. R. Wilkinson, Proc. R. Soc. London, Ser. A **381**, 17 (1982).
[37] M. Kardar, G. Parisi, and Y.-C. Zhang, Phys. Rev. Lett. **56**, 889 (1986).
[38] E. Medina, T. Hwa, M. Kardar, and Y.-C. Zhang, Phys. Rev. A **39**, 3053 (1989).
[39] T. Sun, H. Guo, and M. Grant, Phys. Rev. A **40**, 6763 (1989).
[40] J. Villain, J. Phys. I **1**, 19 (1991).
[41] Z.-W. Lai and S. Das Sarma, Phys. Rev. Lett. **66**, 2348 (1991).
[42] L.-H. Tang and T. Nattermann, Phys. Rev. Lett. **66**, 2899 (1991).
[43] M. D. Johnson, C. Orme, A. W. Hunt, D. Graff, J. Sudijono, L. M. Sander, and B. G. Orr, Phys. Rev. Lett. **72**, 116 (1994).
[44] M. Kotrla and P. Šmilauer, Phys. Rev. B **53**, 13777 (1996).
[45] S. Das Sarma, P. P. Chatraphorn, and Z. Toroczkai, Phys. Rev.

E **65**, 036144 (2002).
[46] S. Pal, D. P. Landau, and K. Binder, Phys. Rev. E **68**, 021601 (2003).
[47] W. Zhu, F. B. de Mongeot, U. Valbusa, E. G. Wang, and Z. Zhang, Phys. Rev. Lett. **92**, 106102 (2004).
[48] A. Ballestad, B. J. Ruck, M. Adamcyk, T. Pinnington, and T. Tiedje, Phys. Rev. Lett. **86**, 2377 (2001).
[49] A. Ballestad, B. J. Ruck, J. H. Schmid, M. Adamcyk, E. Nodwell, C. Nicoll, and T. Tiedje, Phys. Rev. B **65**, 205302 (2002).
[50] F. Buatier de Mongeot, W. Zhu, A. Molle, R. Buzio, C. Boragno, U. Valbusa, E. G. Wang, and Z. Zhang, Phys. Rev. Lett. **91**, 016102 (2003).
[51] C. A. Haselwandter and D. D. Vvedensky, Phys. Rev. Lett. **98**, 046102 (2007).
[52] C. A. Haselwandter and D. D. Vvedensky, Europhys. Lett. **77**, 38004 (2007).
[53] C. A. Haselwandter, Ph.D. thesis, University of London, 2007 (unpublished), available online at http://www.imperial.ac.uk/research/cmth/research/theses.
[54] C. A. Haselwandter and D. D. Vvedensky, Phys. Rev. E **76**, 041115 (2007).
[55] D. D. Vvedensky, A. Zangwill, C. N. Luse, and M. R. Wilby, Phys. Rev. E **48**, 852 (1993).
[56] Alvin L.-S. Chua, C. A. Haselwandter, C. Baggio, and D. D. Vvedensky, Phys. Rev. E **72**, 051103 (2005).
[57] F. Family, J. Phys. A **19**, L441 (1986).
[58] S. Pal and D. P. Landau, Physica A **267**, 406 (1999).
[59] A. Röthlein, F. Baumann, and M. Pleimling, Phys. Rev. E **74**, 061604 (2006); **76**, 019901(E) (2007).
[60] D. E. Wolf and J. Villain, Europhys. Lett. **13**, 389 (1990).
[61] S. Clarke and D. D. Vvedensky, Phys. Rev. B **37**, 6559 (1988).
[62] P. Šmilauer and M. Kotrla, Phys. Rev. B **49**, 5769 (1994).
[63] M. R. Wilby, D. D. Vvedensky, and A. Zangwill, Phys. Rev. B **46**, 12896(R) (1992).
[64] M. Schneider, A. Rahman, and I. K. Schuller, Phys. Rev. Lett. **55**, 604 (1985).
[65] M. Schneider, I. K. Schuller, and A. Rahman, Phys. Rev. B **36**, 1340 (1987).
[66] A. F. Voter, in *Proceedings of the NATO Advanced Study Institute on Radiation Effects in Solids*, edited by K. E. Sickafus, E. A. Kotomin, and B. P. Uberuaga (Springer-Verlag, Berlin, 2007).
[67] J. D. Weeks and G. H. Gilmer, Adv. Chem. Phys. **40**, 157 (1979).
[68] N. G. van Kampen, *Stochastic Processes in Physics and Chemistry*, 2nd ed. (North-Holland, Amsterdam, 1992).
[69] G. R. Jafari, S. M. Fazeli, F. Ghasemi, S. M. Vaez Allaei, M. R. Tabar A. Iraji Zad, and G. Kavei, Phys. Rev. Lett. **91**, 226101 (2003).
[70] A. Zangwill, *Physics at Surfaces* (Cambridge University Press, Cambridge, England, 1988).
[71] C. Haselwandter and D. D. Vvedensky, J. Phys. A **35**, L579 (2002).
[72] P. Šmilauer, M. R. Wilby, and D. D. Vvedensky, Phys. Rev. B **47**, 4119 (1993).
[73] M. Siegert and M. Plischke, Phys. Rev. E **50**, 917 (1994).
[74] T. G. Kurtz, J. Appl. Probab. **8**, 344 (1971).
[75] T. G. Kurtz, J. Chem. Phys. **57**, 2976 (1972).
[76] T. G. Kurtz, Math. Prog. Stud. **5**, 67 (1976).
[77] T. G. Kurtz, Stochastic Proc. Appl. **6**, 223 (1978).
[78] W. Horsthemke and L. Brenig, Z. Phys. B **27**, 341 (1977).
[79] W. Horsthemke, M. Malek-Mansour, and L. Brenig, Z. Phys. B **28**, 135 (1977).
[80] P. Hänggi, Z. Phys. B **30**, 85 (1978).
[81] R. F. Fox and J. Keizer, Phys. Rev. A **43**, 1709 (1991).
[82] Comment by W. Horsthemke following the talk by R. Graham, in *Proceedings of the XVIIth International Solvay Conference on Physics*, edited by G. Nicolis, G. Dewel, and J. W. Turner (Wiley, New York, 1981), pp. 282–286.
[83] C. Baggio, R. Vardavas, and D. D. Vvedensky, Phys. Rev. E **64**, 045103(R) (2001).
[84] C. A. Haselwandter and D. D. Vvedensky, Mater. Res. Soc. Symp. Proc. **859E**, JJ8.8.1 (2005).
[85] C. A. Haselwandter and D. D. Vvedensky, Phys. Rev. E **73**, 040101(R) (2006).
[86] M. Předota and M. Kotrla, Phys. Rev. E **54**, 3933 (1996).
[87] C. Ratsch, M. F. Gyure, S. Chen, M. Kang, and D. D. Vvedensky, Phys. Rev. B **61**, R10598 (2000).
[88] C. A. Haselwandter and D. D. Vvedensky, Phys. Rev. B **74**, 121408(R) (2006).
[89] D. D. Vvedensky, Phys. Rev. E **67**, 025102(R) (2003).
[90] J. Aarts, W. M. Gerits, and P. K. Larsen, Appl. Phys. Lett. **48**, 931 (1986).
[91] W. F. Egelhoff, Jr. and I. Jacob, Phys. Rev. Lett. **62**, 921 (1989).
[92] S. C. Wang and G. Ehrlich, Phys. Rev. Lett. **70**, 41 (1993).
[93] G. L. Kellogg, Phys. Rev. Lett. **76**, 98 (1996).
[94] Z. Zhang and H. Metiu, Surf. Sci. **245**, 353 (1991).
[95] C. M. Gilmore and J. A. Sprague, Phys. Rev. B **44**, 8950 (1991).
[96] J. W. Evans, D. E. Sanders, P. A. Thiel, and A. E. DePristo, Phys. Rev. B **41**, 5410 (1990).
[97] Wolfram Research, Inc., Urbana-Champaign, IL, version 5.0.
[98] D. D. Vvedensky, Phys. Rev. E **68**, 010601(R) (2003).
[99] T. S. Chang, D. D. Vvedensky, and J. F. Nicoll, Phys. Rep. **217**, 279 (1992).
[100] S. Clarke, M. R. Wilby, and D. D. Vvedensky, Surf. Sci. **255**, 91 (1991).
[101] M. C. Bartelt and J. W. Evans, Phys. Rev. B **46**, 12675 (1992).
[102] J. G. Amar and F. Family, Phys. Rev. Lett. **74**, 2066 (1995).
[103] C. Ratsch, P. Šmilauer, A. Zangwill, and D. D. Vvedensky, Surf. Sci. **329**, L599 (1995).
[104] C. Ratsch, P. Šmilauer, D. D. Vvedensky, and A. Zangwill, J. Phys. I **6**, 575 (1996).
[105] M. Meixner, R. Kunert, and E. Schöll, Phys. Rev. B **67**, 195301 (2003).
[106] G. Russo and P. Smereka, J. Comput. Phys. **214**, 809 (2006).
[107] A. A. Golovin, S. H. Davis, and P. W. Voorhees, Phys. Rev. E **68**, 056203 (2003).